Characterization of the Bubblegum acyl-CoA synthetase of Microchloropsis gaditana

Elodie Billey, Leonardo Magneschi, Sébastien Leterme, Mariette Bedhomme, Amélie Andres-Robin, Laurent Poulet, Morgane Michaud, Giovanni Finazzi, Renaud Dumas, Serge Crouzy, et al.

Short title

M. gaditana Bubblegum acyl-CoA synthetase

Title

Characterization of the Bubblegum acyl-CoA synthetase of *Microchloropsis gaditana*

Authors

Elodie Billey[1,2], Leonardo Magneschi[1], Sébastien Leterme[1], Mariette Bedhomme[1,2], Amélie Andres-Robin[1], Laurent Poulet[1], Morgane Michaud[1], Giovanni Finazzi[1], Renaud Dumas[1], Serge Crouzy[3], Frédéric Laueffer[2], Laurent Fourage[2], Fabrice Rébeillé[1], Alberto Amato[1], Séverine Collin[2], Juliette Jouhet[1,*], Eric Maréchal[1,*]

Affiliations:

[1]Laboratoire de Physiologie Cellulaire et Végétale, Unité mixte de recherche 5168 CNRS - CEA - INRA – Univ. Grenoble Alpes, Institut de Biosciences Biotechnologies de Grenoble, CEA Grenoble, 17 rue des Martyrs, 38054, Grenoble Cedex 9, France.

[2]Total Raffinage-Chimie, Tour Coupole, 2 Place Jean Millier – 92078 Paris La Défense, France

[3]Laboratoire de Chimie et Biologie des Métaux, Unité mixte de recherche 5249 CNRS - CEA - Univ. Grenoble Alpes, Institut de Biosciences Biotechnologies de Grenoble, CEA Grenoble, 17 rue des Martyrs, 38054, Grenoble Cedex 9, France.

Corresponding Author : Eric Marechal, eric.marechal@cea.fr

* Senior Authors: juliette.jouhet@cea.fr; eric.marechal@cea.fr

One sentence summary

A heterokont Bubblegum acyl-CoA synthetase (ACSBG), or lipidosin, is essential in *Microchloropsis* (*Nannochloropsis*) *gaditana* and thio-esterifies 16:1 and 18:3 fatty acids to Coenzyme A *in vivo.*

List of author contributions:

E.B., L.M., S.L., M.B., L.P., A.A., S.Co. performed molecular biology experiments and genetic and phenotypic studies; A.A.R. contributed to growth experiments in multiple devices and contributed to phenotypic analyses; M.M and G.F provided specific expertise in metabolic and physiologic analyses; F.R. and J.J. provided specific expertise in lipidomic analyses; E.B., R.D. and S.Cr. performed bioinformatic and modeling analyses; E.B., L.F., F.L., S.Co., J.J. and E.M. participated to the conception of research plans; J.J and E.M. conceived the project; all the authors contributed to the writing of the article.

Keywords:

Bubblegum Acyl-CoA synthase; lipidosin; *Nannochloropsis*, *Microchloropsis*; eicosapentaenoic acid; very-long-chain polyunsaturated fatty acid; omega pathway

Abstract

The metabolic pathways of glycerolipids are well described in cells containing chloroplasts limited by a two-membrane envelope but not in cells containing plastids limited by four membranes, including heterokonts. Fatty acids (FAs) produced in the plastid, palmitic and palmitoleic acids (16:0 and 16:1), are used in the cytosol for the synthesis of glycerolipids via various routes, requiring multiple acyl-Coenzyme A (CoA) synthetases (ACS). Here, we characterized an ACS of the Bubblegum subfamily in the photosynthetic eukaryote *Microchloropsis gaditana*, an oleaginous heterokont used for the production of lipids for multiple applications. Genome engineering with TALE-N allowed the generation of MgACSBG point mutations, but no knockout was obtained. Point mutations triggered an overall decrease of 16:1 in lipids, a specific increase of unsaturated 18-carbon acyls in phosphatidylcholine and decrease of 20-carbon acyls in the betaine lipid diacylglyceryl-trimethyl-homoserine. The profile of acyl-CoAs highlighted a decrease in 16:1-CoA and 18:3-CoA. Structural modeling supported that mutations affect accessibility of FA to the MgACSBG reaction site. Expression in yeast defective in acyl-CoA biosynthesis, further confirmed that point mutations affect ACSBG activity. Altogether, this study supports a critical role of heterokont MgACSBG in the production of 16:1-CoA and 18:3-CoA. In *M. gaditana* mutants, the excess saturated and monounsaturated FAs were diverted to triacylglycerol, thus suggesting strategies to improve the oil content in this microalga.

Introduction

In photosynthetic eukaryotes, the glycerolipid composition of subcellular membranes is specific to each compartment; it results from the combination of biosynthetic pathways, located mainly at the chloroplast and the endoplasmic reticulum (ER), and an intense trafficking of lipid intermediates within the cell (Benning, 2008, 2009; Li-Beisson et al., 2010; Boudiere et al., 2012; Horn and Benning, 2016; Li-Beisson et al., 2017; LaBrant et al., 2018; Li-Beisson et al., 2019). Glycerolipids result from the combination of three types of building blocks, *i.e.* a glycerol backbone originating from glycerol-3-phosphate (G3P, each carbon being numbered as *sn*-1, *sn*-2 and *sn*-3), fatty acids (FAs) of different carbon chain lengths and desaturation levels (indicated for instance as 18:1 for 18 carbons and 1 double bond) and polar heads of various chemical structures (Supplemental Fig. S1).

The metabolic pathways are well described in cells containing chloroplasts limited by a two-membrane envelope (so-called 'primary plastids' in Archaeplastida). A gap of knowledge needs to be filled in cells containing plastids limited by four membranes ('secondary plastids' in various clades, including heterokonts) (Petroutsos et al., 2014; Li-Beisson et al., 2019).

In Archaeplastida, such as plants or green algae, *de novo* synthesis of FAs bound to acyl carrier proteins (ACPs) occurs in the stroma of chloroplasts, generating acyl-ACPs, mainly palmitoyl- and stearoyl-ACP (16:0-ACP and 18:0-ACP), which can be desaturated by a stromal acyl-ACP desaturase (AAD), producing 16:1-ACP and/or 18:1-ACP. Acyl-ACPs can be directly used to esterify G3P at the inner envelope membrane of the plastid for the production of precursors for the four major chloroplast glycerolipids, *i.e.* three classes of glycoglycerolipids (monogalactosyldiacylglycerol, MGDG; digalactosyldiacylglycerol, DGDG and sulfoquinovosyldiacylglycerol, SQDG) and one phosphoglycerolipid, (phosphatidylglycerol, PG) (Li-Beisson et al., 2010; Boudiere et al., 2014). Chloroplasts also export FAs and import glycerolipid precursors: acyl-ACPs can be converted into free FAs

(FFAs) by a chloroplast-specific thioesterase; FFAs then move to the cytosol, where they are thioesterified to Co-enzyme A (CoA), thus forming acyl-CoAs (Li et al., 2015; Li et al., 2016; Li-Beisson et al., 2017). This thioesterification is catalyzed by acyl-CoA synthetases (ACSs), acting therefore in the control of FA fluxes in the cytosol, and their sorting toward different end-products (Coleman et al., 2002; Mashek et al., 2006; Mashek et al., 2007). Acyl-CoAs are acyl donors for the formation of the initial precursors for all membrane phosphoglycerolipids in the ER, like phosphatidylcholine (PC) or phosphatidylethanolamine (PE), or for triacylglycerol (TAG) stored in lipid droplets (Li-Beisson et al., 2010).

Superimposed to this glycerolipid biosynthetic network, FAs can be 'removed' from a given glycerolipid by specific lipases, releasing FFAs, and be replaced by the action of specific acyl-CoA-dependent acyltransferases. This process is known as 'acyl editing' (Bates et al., 2012; Hurlock et al., 2018; Menard et al., 2018). The pool of acyl-CoAs can be used for the elongation of FAs by specific elongases and the synthesis of other acylated molecules, such as sterol-esters or acyl-proteins. Eventually, acyl-CoAs can be directed to catalytic organelles, such as mitochondria or peroxisomes, to be specifically degraded by a process known as beta-oxidation (Pei et al, 2003).

It is difficult to deduce the precise cellular function of ACSs, since they can be essential in the activation of *de novo* synthesized FAs as well as recycled ones, for a broad diversity of 'acyl-CoA-dependent' purposes (Fig. 1). Some ACSs operate in more than one pathway (Coleman et al., 2002; Mashek et al., 2006; Mashek et al., 2007). The function of each ACS depends therefore on multiple parameters, including substrate specificity, temporal expression pattern, location within the cell, interaction with other proteins, etc. Genetic impairment of *ACS* genes appears therefore as a method of choice to address functionality.

By contrast with Archaeplastida, Heterokonta contain a plastid with four limiting membranes (Fussy and Obornik, 2018). In models such as the diatom *Phaeodactylum tricornutum* or the

eustigmatophytes *Microchloropsis gaditana* and closely related species such as *Nannochloropsis oceanica*, the *two innermost* membranes of the secondary plastid are considered homologous to the two-membrane envelope of plant chloroplasts (the inner and outer envelope membranes, IEM and OEM respectively). The *outermost membrane*, the epiplastid membrane (EpM), is continuous with the outer nuclear envelope membrane connected to the ER. The periplastid membrane (PpM) located between the EpM and the OEM is of a still unresolved origin (Flori et al., 2016; Cavalier-Smith, 2018). The glycerolipid biosynthetic scheme seems to follow some rules deciphered in plants, i.e. (1) a *de novo* synthesis of FAs up to C16 in the stroma, generating 16:0-ACP, (2) the presence of enzymes involved in MGDG, DGDG and SQDG biosynthesis probably located in plastid membranes and (3) the presence of enzymes involved in phospholipid synthesis, such as PC and PE, probably located in the ER (Petroutsos et al., 2014; Abida et al., 2015; Dolch and Marechal, 2015; Dolch et al., 2017). Photosynthetic heterokonts contain an additional glycerolipid class, the betaine lipids, whose synthesis is usually associated with the ER. In *P. tricornutum* the betaine lipid is diacylglyceryl-3-O-2'-(hydroxymethyl)-(N,N,N-trimethyl)-β-alanine (DGTA) (Abida et al., 2015), whereas *M. gaditana* or *N. oceanica* contain diacylglyceryl-3-O-4'-(N,N,N-trimethyl)-homoserine (DGTS) (Alboresi et al., 2016; Dolch et al., 2017; Murakami et al., 2018).

Besides these general features, essential differences make it extremely challenging to transfer knowledge acquired in plant or green algal models to Heterokonta:

- Firstly, after *de novo* synthesis in the plastid, 16:0 is exported to the cytosol, where it is thioesterified into 16:0-CoA. This 16:0-CoA is the initial substrate for a series of elongations and desaturations forming at first 18:0-CoA and ending up with very-long-chain polyunsaturated fatty acids (VLC-PUFAs) in the ER, such as eicosapentaenoic acid (EPA or 20:5) (Dolch et al., 2017). Since elongations operate on acyl-CoAs,

whereas desaturations occur on acyl-glycerolipids, the 16:0-to-20:5 route requires five classes of enzymes, i.e. specific ACSs to supply elongases and acyl-transferases with activated FAs, desaturases acting on a "glycerolipidic platforms" harboring the acyl-group, where double bonds are added, and lipases A (Fig. 1). In *P. tricornutum* and *M. gaditana*, based on the detection of 16:0-to-20:5 intermediates (mainly 18:0, 18:1, 18:2, 18:3, 20:3 and 20:4), the most likely glycerolipid plaftorms for 20:5 biosynthesis are PC and the betaine lipid (Abida et al., 2015; Dolch et al., 2017; Sayanova et al., 2017).

- Secondly, 16:0-ACP is presumed to be desaturated into 16:1-ACP in the plastid. Palmitoleic acid is exported to the cytosol, where it is thioesterified into 16:1-CoA. Palmitoleoyl-CoA is the preferred substrate for one of the four lysophosphatidic acyltransferases occurring in *N. oceanica*, i.e. LPAT1, residing in the ER and adding 16:1 at position *sn*-2 of membrane glycerolipids, mainly PC and DGTS (Nobusawa et al., 2017).
- Eventually, DGTS, MGDG and DGDG are marked by an extremely high content in 20:5 (Botte et al., 2011; Abida et al., 2013; Alboresi et al., 2016; Dolch et al., 2017; Murakami et al., 2018). Genetic knock out of enzymes producing DGTS in *N. oceanica* showed that this betaine lipid was a pool of 20:5 in the cytosol, where 20:5 is actually synthesized (Murakami et al., 2018). To accumulate into MGDG and DGDG, 20:5 needs to relocate from the ER to the plastid, a process unlikely to be homolog of the "eukaryotic pathway" described in Arabidopsis (*Arabidopsis thaliana*). This import of 20:5 to the plastid of heterokonts has been termed the "omega pathway" (Petroutsos et al., 2014; Dolch et al., 2017). Based on the genetic knock out of the elongase *Δ0-elo1* in *M. gaditana*, the omega pathway seems to operate via a large-scale multi-enzymatic and multi-site channeling machinery, starting from the initial

elongation of 16:0-CoA into 18:0-CoA by a Δ0-ELO isoform in the ER, and ending by the formation of 20:5 and its transfer to MGDG in the plastid (Dolch et al., 2017).

In heterokonts, ACS isoforms are therefore expected to operate in FA fluxes at all these steps. We have focused our study on *M. gaditana*, previously known as *Nannochloropsis gaditana* (Fawley et al., 2015). *Microchloropsis* and *Nannochloropsis* are oleaginous microalgae, producing high levels of TAG and representing therefore a promising feedstock for biofuel and green chemistry, motivating important efforts into optimizing strains and culture conditions (Van Vooren et al., 2012; Camacho-Rodriguez et al., 2013; Chen et al., 2013; Camacho-Rodriguez et al., 2014; Ma et al., 2014; Camacho-Rodriguez et al., 2015; Meng et al., 2015) and developing genetic engineering methods (Radakovits et al., 2012; Vieler et al., 2012; Iwai et al., 2015; Kang et al., 2015; Dolch et al., 2017; Poliner et al., 2018). *M. gaditana* is a model where C18 desaturation occurs mainly on PC, whereas C20 desaturations occur mainly on DGTS and PE (Alboresi et al., 2016). To our knowledge, no genetic study has focused on *ACS* genes in heterokonts. We addressed the role of an ACS isoform in *M. gaditana* belonging to the Bubblegum subfamily (ACSBG) (Min and Benzer, 1999; Steinberg et al., 2000; Pei et al., 2003; Mashek et al., 2007; Song et al., 2007; Lopes-Marques et al., 2018) by genome engineering with tailored TALE-N.

Results and Discussion

Identification of an Acyl-CoA synthetase of the « Bubblegum » subfamily (ACSBG) in *M. gaditana*

We sought ACS genes that could be distinct between Heterokonta and Archaeplastida. The genome of *M. gaditana* contains six genes annotated as Acyl-CoA synthetases (*ACS*) or Acyl-CoA ligases (*ACL*): Naga_100014g59; Naga_100012g66; Naga_101051g1; Naga_100047g8; Naga_100649g1 and Naga_100035g43 (http://protists.ensembl.org/Nannochloropsis_gaditana_gca_000569095/). The genome of the model diatom *P. tricornutum* contains five putative *ACS* genes: Phatr3_J20143 (annotated as *ACS1*), Phatr3_J12420 (*ACS2*), Phatr3_J54151 (*ACS3*), Phatr3_J45510 (*ACS4*) and Phatr3_J17720 (*ACL1*) (http://protists.ensembl.org/Phaeodactylum_tricornutum). In the current state of knowledge, it is not possible to predict the specificity of a given ACS sequence for FAs.

Based on protein sequences, subfamilies of eukaryote ACSs have been defined (Steinberg et al., 2000; Watkins et al., 2007). One subfamily corresponds to the “Bubblegum” Acyl-CoA synthetases (ACSBG), named after the bubbly appearance of the first optic ganglion induced by the mutation of the corresponding gene in the fruit fly *Drosophila melanogaster*, leading to a neurodegeneration and elevated level of VLC-FAs (Min and Benzer, 1999). ACSBGs are also called “lipidosins” (Song et al., 2007). ACSBGs have been mainly studied in Metazoa, conserved from invertebrates to vertebrates (Lopes-Marques et al., 2018). The impairment of *ACSBG* in *Drosophila* or mice leads to an increase of VLC-PUFAs, however the beta-oxidation of VLC-PUFAs that could partly explain this increase seems not always affected in corresponding *acsbg* mutants (Min and Benzer, 1999; Steinberg et al., 2000; Song et al., 2007). The human (*Homo sapiens*) *ACSBG1* gene is expressed primarily in the brain (Steinberg et al., 2000). Brains have higher concentrations of VLC-FAs than other tissues,

including VLC-PUFAs like 20:5 and 22:6; these VLC-FAs are components of complex lipids such as gangliosides, cerebrosides, sulfatides, sphingomyelin and other phospholipids, all kinds of lipids whose synthesis could also rely on ACSBG (Steinberg et al., 2000). The specific expression of *ACSBG* gene in animal brains as well as biochemical studies show that ACSBG proteins are involved in the activation of PUFAs and VLC-PUFAs, with chain lengths from 16 to at least 24 carbons (Steinberg et al., 2000). Concerning the two genes in human, although *ACSBG1* was initially thought to activate VLC-FAs based on overexpression studies (Steinberg et al., 2000), investigation of the endogenous enzyme using RNA interference highlighted a high specificity for C16:0 (Pei et al., 2003). By contrast, *ACSBG2* preferentially activates C18:1 and C18:2 acids (Watkins et al., 2007). In chicken, a single nucleotide polymorphism in the *ACSBG2* gene is associated with abdominal fat weight and percentage (Claire D'Andre et al., 2013). ACSBG proteins contain conserved domains, among which motif II is possibly involved in FA-binding (Moriya-Sato et al., 2000; Steinberg et al., 2000; Watkins et al., 2007; Lopes-Marques et al., 2018). Based on the conservation of motif II (Fig. 2), we identified ACS isoforms of the bubblegum type in *M. gaditana* (*MgACSBG*; Naga_100014g59) and *P. tricornutum* (annotated as *ACS4* and called here *PtACSBG*; Phatr3_J45510). MgACSBG and PtACSBG share five conserved ACSBG motifs (Lopes-Marques et al., 2018), further confirming their structural identification as ACSBG (Supplemental Fig. S2).

We compared ACS sequences found in *M. gaditana* and *P. tricornutum* with sequences of previously characterized ACSBG in animals, *i.e. D. melanogaster* (DmACSBGa, NP_524698; DmACSBGc, NP_001285923); *Homo sapiens* (HsACBG1, Q96GR; HsACBG2, Q5FVE4); *Mus musculus* (MmACSBG1, NP_444408); *Gallus gallus* (GgACSBG1, F1NLD6; GgACSBG2, XP_015155301). Our Bayesian phylogenetic analysis showed a robustly supported clade (posterior probability 1.00) grouping *M. gaditana* and *P. tricornutum*

ACSBG with metazoan bubblegum/lipidosin sequences. The other algal ACS sequences grouped in separate clades (Fig. 3).

Using the MgACSBG sequence as query, and based on (1) similarity search using BlastP, with a Blosum 62 similarity matrix, default parameters and an e-value threshold of 1×10^{-10}, and (2) detection of a conserved motif II, we could identify ACSBG homologues in both photosynthetic (e.g. *Ectocarpus*, CBJ33608 or *Fistulifera*, GAX09496) and non-photosynthetic (e.g. *Pithyum*, GAX99969 or *Phytophtora*, XP_008898610) heterokonts. By contrast, we could not identify any sequence in Arabidopsis nor in any plant (Embryophyta). Likewise, no ACSBG homologue could be found in the green alga model *Chlamydomonas reinhardtii.* Nevertheless, some green algae, such as *Ostreococcus tauri* or *Micromonas pusilla*, contained *ACSBG* genes, i.e. XP_003083453 and XP_003061097, respectively. Since *Ostreococcus* differs from *Chlamydomonas* by its ability to produce high levels of VLC-PUFAs up to 22:6 (Degraeve-Guilbault et al., 2017), the presence of an ACSBG might be related to VLC-PUFA fluxes within the cell. We addressed the function of this class of heterokont ACSBG in *M. gaditana*.

TALE-N generation of *M. gaditana acsbg* mutants

We sought to introduce mutations in the *MgACSBG* gene using a specifically designed transcription activator-like effector nuclease (TALE-N), a method with high target binding specificity compared to other gene-editing systems (Malzahn et al., 2017) and with the possibility to generate different types of mutations, ranging from in-frame residue substitutions to gene interruption and knock out (Ma et al., 2016). The target site for TALE-N mutation in *MgACSBG* was selected by comparison with the whole genome to avoid multiple binding of the nuclease. The TALE-N target site was located at the beginning of the coding sequence to allow the generation of incomplete and inactive proteins. This region encodes a

hydrophobic domain of the protein, which might be important for the correct folding of the protein, but distinct from ACSBG conserved motifs. Sequences coding for the two TALE-N binding subunits (Tal2Ng-L and Talg2Ng-R) were designed as described in the Methods section, to position the FokI DNA cleavage domain at the target site (Fig. 4, A), and they were cloned in two independent vectors, pCT61 and pCT62, respectively. Following *M. gaditana* co-transformation with pCT61 and pCT62 and selection on zeocin, obtained colonies were firstly analyzed by treatment of PCR amplified target locus with a T7 endonuclease to detect cleaved DNA at mismatched positions and assess the occurrence of genome editing. To define precisely how the TALE-N modified the target DNA site, cells from T7-positive colonies were sub-cloned onto a new selective plate to separate cells harboring the mutation from those containing wild-type (WT)-like sequences.

Seven T7-positive lines were obtained from multiple independent co-transformations with the pCT61 and pCT62 plasmids. No disruption of the *MgACSBG* full length coding sequence could be obtained, suggesting that knockout (KO) might be lethal. Only nucleotidic modifications leading to in-frame amino acid substitutions could be obtained (Fig. 4, A). In some of the *M. gaditana* transformed lines, e.g. MgACSBG#5, MgACSBG#31 and MgACSBG#40, TALE-N activity led to in-frame insertions/deletions and introduction of non-synonymous codons, leading to point mutant proteins (Fig. 4, B).

In vivo *impact of MgACSBG#5 and MgACSBG#31 in-frame mutations on glycerolipid profiles*

We focused our phenotype analyses on two in-frame mutations, MgACSBG#5 and MgACSBG#31. Cells were cultivated in parallel in a nutrient-rich liquid medium, using a Multicultivator photobioreactor, supplied with CO_2 as described in the Methods section. Control strains consisted of untransformed cells (wild type, WT) and cells transformed with an empty vector (EV). Experiments were performed in duplicate for each line and were

repeated to obtain data from independent replicates (n = 4). The MgACSBG#5 and MgACSBG#31 lines showed a slower growth compared to WT and EV strains, monitored by cell counting at day 3, 7 and 12 following inoculation (D3, D7 and D12, respectively) (Fig. 5, A). Compared to WT and EV strains, the total FA content per cell was higher in the MgACSBG#31 mutant in the early stage of cultivation (D3) (Fig. 5, B), reflecting a higher content in TAG (Fig. 5, C). WT and EV strains showed an accumulation of TAG at D7 and D12 induced by the shortage of nutrients in the medium, as described earlier (Simionato et al., 2013; Alboresi et al., 2016) (Fig. 5, C). MgACSBG#5 and MgACSBG#31 mutants also showed increased TAG content at D7 and D12, but the difference with WT and EV strains was less pronounced, probably due to the nitrogen starvation.

We focused our comparison of MgACSBG#5 and MgACSBG#31 with WT and EV cells at D3, when no starvation of nutrients occurs. The total FA profile of mutant lines showed an increase in 16:0 proportion balanced by a slight decrease in 16:1 in MgACSBG#31 and a significant decrease of 20:5 in one of the mutants (Fig. 5, D). The glycerolipid profile highlighted an increase in TAG and little change in the level of other glycerolipid classes (Fig. 5, E). Since in *M. gaditana* TAG are 16:0-rich and 20:5-poor (Simionato et al., 2013; Alboresi et al., 2016), one could consider that the global increase in 16:0 and the decrease in 20:5 in the mutant lines might simply reflect the accumulation of TAG. We addressed this question by comparing the FA profile of each glycerolipid class at D3.

The comparison of FA profiles in glycerolipid classes in the ACSBG mutants with WT or EV strains showed a striking impact on PC, DGTS and PE (Fig. 6, A-C), synthesized in the ER of *M. gaditana*, and on two of the plastid lipids, MGDG and DGDG (Fig. 6, F-G), whereas little or no significant change could be observed on PG and SQDG (Fig. 6, D-E). In LC-MSMS analyses, m/z spectra correspond to diacyls indicated by the sum of carbons and the number

of double bonds (Alboresi et al., 2016), e.g. in PC, 34-2 corresponds to the major molecular species 16:0/18:2.

We first noticed in the MgACSBG#5 and MgACSBG#31 mutants a decrease of molecular species containing a 16:1 at sn-2 position in PC (e.g. 16:0/16:1; 16:1/16:1) and DGTS (e.g. 14:0/16:1; 16:1/16:1) (Fig. 6, A, B and C). This could reflect a role of ACSBG in producing 16:1-CoA for the *de novo* synthesis of lipids at the ER, reminiscent of the effect of the knockout of LPAT in the closely related species *N. oceanica*, an enzyme shown to transfer 16:1 at the sn-2 position of these lipids (Nobusawa et al., 2017).

These lipids are presumed to also serve as "platforms" for the production of 20:5, *i.e.* PC from 16:0 to 18:3 and DGTS from 20:3 to 20:5. This role is not fully restricted to PC and DGTS: it was shown in *N. oceanica* that mutants lacking DGTS lead to the accumulation of 18:1, 18:2 and 20:4 in PC, consistently with an accumulation of 20:5 precursors in this lipid, and more 20:4 and 20:5 in PE, consistently with PE acting as a secondary platform for the final steps of 20:5 production (Murakami et al., 2018). Here, in MgACSBG#5 and MgACSBG#31, PC molecular species containing 18:1 and 18:2 (16:0/18:1; 16:0/18:2; 16:1/18:2) were enriched, corresponding to an accumulation of 18:3 precursors (Fig. 6, A and Supplemental Table S1). We had a closer look at PC acyl profiles and could detect 18:3 only in MgACSBG#5 and MgACSBG#31 (16:1/18:3, 18:2-18:3 and 18:1/18:3; Supplemental Table S1). In these mutants, DGTS had more diacyls with 16:0 and 18:1 (16:0/16:0; 18:1/16:0; 20:4/16:0; 20:5/16:0) and fewer diacyls containing only 20-carbon FAs (20:4/20:4; 20:5/20:4; 20:5/20:5) (Fig. 6, B). PE was also altered, containing less 20:5 (16:1/20:5; 20:5/20:5) and higher levels of 20:3 and 20:4 (20:4/20:3; 20:5/20:5) (Fig. 6, C). In the MgACSBG#5 and MgACSBG#31 mutants, 18-carbon precursors of 18:3 accumulated in PC (18:0; 18:1; 18:2 and 18:3), and 20:5 proportions decreased in DGTS and PE. This could reflect a role of ACSBG in producing 18:3-CoA in the pathway producing 20:5 in DGTS and to some extent in PE.

The profile of MGDG in the MgACSBG#5 and MgACSBG#31 mutants is characterized, like in the WT, by a major molecular species with a m/z corresponding to 34 carbons and 5 double bonds (34-5 or 20:5/14:0). Little change was observed, besides a decrease of molecular species enriched in 16:1 (16:1/16:0; 16:1/16:1) and a slight increase in 20:5-rich molecular species (20:5/16:0; 20:5/20:5) (Fig. 6, F). DGDG showed the same trend but with a higher magnitude, *i.e.* a dramatic decrease in the proportion of 16:1 (16:1/16:0; 16:1/16:1) compensated by an increase in 20:5 (20:5/14:0, 20:5/16:0; 20:5/16:1) (Fig. 6, G). Since the amount of plastid glycerolipids was either unchanged or slightly decreased in the mutants, the observed phenotype in the MgACSBG#5 and MgACSBG#31 mutants reflected a depletion of 16-carbon FAs, mainly 16:1, partly compensated by imported 20:5.

The profile of TAG in the MgACSBG#5 and MgACSBG#31 mutants was also different from that in the WT and EV lines. It was globally characterized by a decrease in 16:1-rich molecular species (14:1/16:1/16:1; 16:1/16:1/16:0; 16:1/16:1/16:1; 16:1/18:1/16:1) and a higher level of 16:0-rich molecular species (16:0/16:0/16:1; 16:0/16:0/16:0) as well as a noticeable increase in 18:0 and 18:1 (16:1/16:0/18:0 and 16:1/16:0/18:1) (Fig. 6, H).

Altogether, these data indicate that a point mutation in the MgACSBG sequence leads to a modification of FA partitioning within *M. gaditana* cells, altering two pathways, one being the incorporation of 16:1 at the sn-2 position of ER glycerolipids via the LPAT1 pathway dissected in *N. oceanica* (Nobusawa et al., 2017), another being the 16:0-to-20:5 elongation/desaturation process occurring on the PC and DGTS platforms, both leading to an accumulation of 16:0 in ER lipids and TAG and an exhaustion of 16-carbon from plastid glycerolipids.

The lack of KO mutant after TALE-N genetic mutation of MgACSBG suggests that this acyl-CoA transferase operating in two key processes is critical. A possible interpretation is shown in Figure 7, following FA biosynthesis in the plastid (Fig. 7, A), with a first role for ACSBG

in the production of 16:1-CoA in the cytosol (Fig. 7, B), prior to incorporation of 16:1 in ER lipids via the LPAT1 pathway (Nobusawa et al., 2017) (Fig. 7, C). 16:0-CoA also entered the 16:0-to-20:5 channeling process, following a first elongation via a Δ0-ELO producing 18:0-CoA (Fig. 7, D). A second role for ACSBG in the production of 18:3-CoA was also deduced from the mutants' phenotype in PC, DGTS and PE (Fig. 7, E-F). As a result of ACSBG impairment, an over-accumulation of 16:0-CoA was expected and observed (Fig. 7, G). An important assumption for this model is that a positive feedback is exerted on the plastid, exporting most of its FAs, and explaining that the plastid is depleted of its 16-carbon FAs and that the omega pathway is activated to provide sufficient 20:5 compensating the lack of 16-carbon substrates in plastid glycerolipids (Fig. 7, H). In our scheme, the omega pathway appears important for the synthesis of both MGDG and DGDG. The absence of any viable knock-out mutant indicates that no other ACS isoforms from *M. gaditana* could apparently compensate a lack of functional MgACSBG.

Impact of MgACSBG#5 and MgACSBG#31 mutations on acyl-CoA profiles

Acyl-CoAs from WT, EV and mutant cells grown in nutrient replete condition were extracted and sent to Rothamsted Research, UK, for a targeted analysis of chain lengths from 10 to 20 carbons (using 10:0; 12:0; 14:0; 16:0; 16:1; 16:3; 18:0; 18:1; 18:2; 18:3; 18:4; 18:5; 20:0; 20:3; 20:4 and 20:5 standards), as described in the Methods section (Fig. 8). The level of only three acyl-CoAs showed a significant variation in mutants compared to WT, *i.e.* an increase in 16:0-CoA and a decrease in 16:1-CoA and 18:3-CoA. This analysis is consistent with a dual role of ACSBG in the activation of 16:1 and 18:3 into 16:1-CoA and 18:3-CoA. We sought to better comprehend the molecular impact of the mutation introduced in the MgACSBG protein.

Molecular impact of MgACSBG#5 and MgACSBG#31 mutations on the protein structure.

The MgACSBG sequence contains 649 amino acids and is predicted to be soluble with a MW of 71,056 Da. We sought to construct a 3D structural model that could in part provide clues to understand the effects of the mutations at the level of the IGF domain (a triad defined by isoleucine 96, glycine 97 and phenylalanine 98). It seemed essential to propose the positioning of a FA chain in the model, i.e. α-linolenic acid (18:3; $C_{18}H_{30}O_2$ *cis*-Δ9,12,15), as a substrate for MgACSBG deduced from phenotypic analyses. The search of conserved acyl-CoA synthetase motifs was refined *via* the online servers MOTIF (Kanehisa et al., 2002) and PROSITE (Sigrist et al., 2013), which identified an AMP binding motif, while Superfamily (Wilson et al., 2009) confirmed that MgACSBG belonged to an Acetyl-CoA synthetase-like family. The Porter predicting method (Mirabello and Pollastri, 2013) found 44% coil, 37% helix and 19% extended conformation while Predictprotein (Yachdav et al., 2014) gave the secondary structure prediction shown in Supplemental Fig. S3.

The sequence alignment of MgACSBG with 4 proteins used as templates in our models (see below) is shown in Supplemental Fig. S4. The most clearly conserved motif YTSGTTGPPK (residues 216-225), identified as the AMP binding motif, was requalified as playing a fundamental role in ACS catalytic activity (Gulick et al., 2003; Lopes-Marques et al., 2018). The long sequence SITGRIKELIITAGGENIPPVLIE (residues 492-515), or "motif II", contains a part of the "FACS motif" (fatty acyl CoA synthetase signature motif) (Black et al., 1997) and is supposed to be involved in acyl chain length specificity. In ACSBGs, a so-called "motif III" (F/YG-SE) (residues 409-413) has been proposed as being involved in AMP binding, whereas "Motif IV" (LPLSH) (residues 259-263) could be involved in CoA binding (Lopes-Marques et al., 2018).

No structure is currently available for an ACSBG in public databases. The sequence was first submitted to Blast (Altschul et al., 1990) to find sequence alignments with proteins of known 3D structure. The first hit was referenced 1ULT in the Protein Data Bank (PDB, (Burley et

al., 2019)) and corresponds to a long chain fatty acyl-CoA synthetase homodimer from *Thermus thermophilus* (Hisanaga et al., 2004), with 27% sequence identity and 40% homology. Then the sequence was submitted to several online prediction servers (Robetta (Song et al., 2013) ; RaptorX (Kallberg et al., 2012); Swiss-Model (Waterhouse et al., 2018); PhyRe2 (Kelley et al., 2015) ; I-Tasser (Zhang, 2009); PsiPred (Buchan et al., 2013) and PS(2) (Huang et al., 2015)). All methods failed to predict the full MgACSBG protein and most of them found 1PG4 (acetyl-CoA synthetase from *Salmonella enterica*) (Gulick et al., 2003), and 5MSC (the A domain of carboxylic acid reductase from *Nocardia iowensis*) (Gahloth et al., 2017) as templates. Despite its low homology with MgACSBG, another acyl-CoA synthetase with known 3D structure and for which both AMP and CoA are resolved was chosen as template: 3EQ6, a human acyl-CoA synthetase medium-chain family member (Kochan et al., 2009). The sequences of these four template proteins were aligned with MgACSBG in Supplemental Fig. S4.

3D structural homology models of the full length MgACSBG protein were built with Modeller (Sali and Blundell, 1993) using different association of template proteins: M1pg4 from 1PG4 alone, M3eq6 from 3EQ6 alone and two consensus models Mcons1 from 1PG4, 1ULT and 5MSC, and Mcons2 from all four protein templates (Supplemental Models 1 to 4). The positioning of CoA and AMP in the MgACSBG models was based on their neighboring residues in structure 1PG4 and 3EQ6, also identified in animal ACSBG2 (Steinberg et al., 2000) (Supplemental Tables S2) as described in the Methods section. The positioning of 18:3 was placed inside the structures, with the carboxy-terminal “head” in the direction of AMP, respecting its proximity with CoA and profiting of hydrophobic holes observed in the structures.

Three models of MgACSBG, M1pg4, M3eq6 and Mcons1, have similar final energy and correctly respect the restraints. From model Mcons1 of MgACSBG (Fig. 9), the proximity of

the IGF triad, mutated in this study, to the inserted 18:3 FA is clear. Their relative position is globally the same in all models. Our modelling supports therefore the hypothesis that the mutation could affect the accessibility of the FA to the reaction site rather than interfere with the reaction itself through proximity with AMP or CoA.

MgACSBG but not MgACSBG#5 or MgACSBG#31 partially complement a yeast defective in acyl-CoA synthase function.

We sought to decipher whether MgACSBG and its two variants could be active after heterologous expression in the yeast *Saccharomyces cerevisiae* and complement the phenotype of a *faa1Δfaa4Δ* double mutation. In yeast, acyl-CoA can originate from neo-synthesis by a fatty acyl synthase (FAS) or by the activation of exogenous FAs by ACSs (Black and DiRusso, 2007). Faa1 and Faa4 are the major enzymes involved in the formation of long chain fatty acyl-CoA (Johnson et al., 1994). In normal growth condition, the *faa1Δfaa4Δ* mutant does not show any growth defect. However, when yeast FAS is inactivated by the addition of cerulenin, the mutant strain cannot grow, even in the presence of exogenously supplied FAs, due to a low level of acyl-CoA synthetase activity (less than 5% of WT activity) (Johnson et al., 1994; Faergeman et al., 2001). MgACSBG, MgACSBG#5 and MgACSBG#31 were expressed in the yeast *faa1Δfaa4Δ* mutant from a high copy vector under the galactose inducible pGAL1 promoter. The WT and *faa1Δfaa4Δ* strains transformed with the empty vector were used as controls. Control strains will be henceforth referred to as 'yeast WT' and '*faa1Δfaa4Δ* mutant', respectively, for simplicity. All the strains were grown on synthetic media deprived of uracil (-U) and supplemented with galactose 2% for 6 h to induce expression of the transgenes prior to dilution to OD_{600} = 0.3. Growth curves were then performed at 30°C. All the strains used in the complementation experiments were tested for expression of MgACSBG variants by immunoblot (Supplemental

Fig. S5). All strains presented an exponential growth in synthetic medium with galactose but did not grow in the presence of 22.5 µM cerulenin, as expected (Supplemental Fig. S5).

In a first set of experiments, we tested the ability of a series of FAs, namely 14:0, 16:0, 18:0, 18:1, 18:2, and 18:3, to rescue the growth of the yeast WT in presence of cerulenin. In our conditions, 14:0 and 16:0 FAs were able to almost fully complement the growth defect induced by cerulenin, whereas 18:0 and 18:1 only partially did, as previously observed by others (Fig. 10, A) (Johnson et al., 1994; Johnson et al., 1994). Conversely, 18:2 and 18:3 FAs were not able to rescue the growth of yeast WT in presence of cerulenin, likely because these two FAs are not naturally present in yeast.

We next investigated the ability of MgACSBG native sequence to complement the *faa1Δfaa4Δ* strain in presence of cerulenin with the same set of FAs previously tested. Three independent clones were analyzed. The results presented in Figure 10, B show that MgACSBG partially rescued the growth phenotype of the double mutant in presence of C14:0 and C16:0. Altogether, these results provide evidence that MgACSBG has indeed an acyl-CoA synthetase activity, is able to use at least 14:0 or 16:0 but cannot provide more information on the specificity for other FAs. MgACSBG-transformed yeast have the same order of apparent preference for 14:0 and 16:0 as that observed in the wild-type yeast (Fig. 10, A), thus indicating that this method is not suitable to address the question of the substrate specificity of MgACSBG at the molecular level.

In the light of the results presented above, 14:0 and 16:0 were retained for further investigation. The same experiments were performed with three independent clones expressing MgACSBG#5 and MgACSBG#31 in a *faa1Δfaa4Δ* background in presence of cerulenin and 14:0 or 16:0. Neither MgACSBG#5 nor MgACSBG#31 (Figs 10, C-D; Supplemental Fig S5, C-E) were able to complement the growth phenotype of the mutant strains in presence of 14:0 and 16:0, unlike MgACSBG. Altogether, these results indicate that

the TALE-N generated mutations interfered with the acyl-CoA synthetase activity of MgACSBG, and that this decline in activity was related with the observed phenotype in in *M. gaditana*.

Conclusion and perspectives.

ACS enzymes generate acyl-CoA pools at different locations of the cell, of different FA profiles and for specific acylation reactions. They are therefore key actors of FA partitioning in lipid metabolism. Unraveling an ACS specific role is made difficult by the possibility of multiple isoforms to compensate a defective enzyme. In photosynthetic eukaryotes, ACS are therefore expected to operate in important acyl fluxes, most importantly from the plastid to the cytosol and vice versa. Heterokonta are marked by the production of VLC-PUFAs in the cytosol, rapidly transferred to the secondary plastid by a channeled processed called the omega pathway. ACS isoforms are expected to operate at 'strategic' levels in this metabolon, in particular after release of 18:3-FFA following acyl desaturation on PC, to generate 18:3-CoA for elongation into 20:3-CoA, precursor for further desaturations on DGTS and/or PE to generate eicosapentaenoic acid, 20:5. Our functional analyses of the *M. gaditana* Bubblegum ACS showed that this enzyme was likely vital, since no KO could be obtained, and that a functional defect impaired two critical steps of acyl-lipid metabolism, the activation of palmitoleic acid, generating 16:1-CoA used to acylate the sn-2 position of ER lipid, and of linolenic acid, generating 18:3-CoA used as intermediate in the 16:0-to-20:5 synthetic process. The obtained mutants using TALE-N editing still contain 20:5, probably because the level of this VLC-PUFA cannot fall below a critical threshold necessary for *M. gaditana* survival. Our results do not exclude that the Heterokont ACSBG also acts in other cellular locations, for other purposes. In a recent study, the *P. tricornutum* homologue, PtACSBG/ACS4, was found in the proteome of the lipid droplet (Lupette et al., 2019), indicating a possible role in the acyl-CoA pool closely associated to this cytosolic organelle. Future works will include the study of this enzyme's location within *M. gaditana*, which is a challenging task given the small size of this microalga. The search of protein partners is also an important perspective, to evaluate the possible association with LPAT1 acting on ER lyso-

lipids, or other components of the machinery converting 16:0 into 20:5 (such as Δ0-ELOs, ERΔFAD9, ERΔFAD12, a PC-specific phospholipase A, Δ5-ELOs, ERΔ5FAD, ERω3FAD, a DGTS/PE-specific lipase A, and subunits of a still-to be identified carrier/transporter importing a 20:5-precursor inside the secondary plastid), or any other protein component that could further highlight the full range of function of this type ACS in a photosynthetic eukaryote.

Materials and methods

MgACSBG phylogenetic analysis.

All genes annotated as acyl-CoA synthetases or ligases from *Microchloropsis gaditana* (Naga_100014g59, MgACSBG; Naga_100012g66; Naga_101051g1; Naga_100047g8; Naga_100649g1 and Naga_100035g43) and *Phaeodactylum tricornutum* (Phatr3_J20143, ACS1; Phatr3_J12420, ACS2; Phatr3_J54151, ACS3; Phatr3_J45510, PtACSBG or ACS4; and Phatr3_J17720, ACL1) were retrieved from public databases, http://protists.ensembl.org/Nannochloropsis_gaditana_gca_000569095/ and http://protists.ensembl.org/Phaeodactylum_tricornutum, respectively. These sequences were compared with ACSBG sequences from Metazoa, *i.e. Drosophila melanogaster* (DmACSBGa, NP_524698; DmACSBGc, NP_001285923); *Homo sapiens* (HsACBG1, Q96GR2; HsACBG2, Q5FVE4); *Mus musculus* (MmACSBG1, NP_444408) and *Gallus gallus* (GgACSBG1, F1NLD6; GgACSBG2, XP_015155301). A phylogenetic tree was reconstructed after a multiple alignment of sequences using the MUSCLE method (v3.8.31) configured for high accuracy with default settings (Edgar, 2004), removal of gaps and poorly aligned sequences using Gblock (Castresana, 2000). The tree was calculated using the phylogeny.fr internet platform (Dereeper et al., 2008) using a Bayesian inference method implemented in the MrBayes program (v3.2.6), with a number of substitution types fixed to 6, a Poisson model for amino acid substitutions, four Markov chain Monte Carlo chains run for 10,000 generations, sampling every 10 generations, discard of the first 250 trees sampled and a 50% majority rule consensus tree (Huelsenbeck and Ronquist, 2001; Ronquist et al., 2012).

Cultivation of M. gaditana *cells*

M. gaditana Strain CCMP526 was used in all experiments. For nuclear transformation, cells were grown under constant light in f/2 medium (Dolch et al., 2017) until they reached the late exponential phase. All cultures were maintained on f/2 plates solidified with 1% agar, w/v,

under a 12:12 light/dark regime in presence (transformed strains) or absence (wild-type strain) of the selective antibiotic zeocin (7 $\mu g \cdot mL^{-1}$). For phenotypic analyses, *M. gaditana* was cultivated in artificial seawater (ESAW) using ten times enriched nitrogen and phosphate sources (5.49 x 10^{-3} M $NaNO_3$ and 2.24 x 10^{-4} NaH_3PO_4; called "10X ESAW") (Dolch et al., 2017). When grown in batch in 250 mL flasks, a volume of 50 mL liquid medium was inoculated at 2.5 × 10^6 cells$\cdot mL^{-1}$ and cultivation was achieved under gentle agitation (100 RPM) at 20°C on a 12:12 light (60 µmol photons$\cdot m^{-2} \cdot s^{-1}$) / dark cycle. When grown with a controlled CO_2 supply, a volume of 80 mL liquid medium was inoculated at 2.5 × 10^6 cells.mL^{-1} and cultivation was achieved in small photobioreactors (Multi-Cultivator MC 1000, Photon Systems Instruments, Czech Republic) at 24°C, in continuous light (illumination at 60 µmol photons$\cdot m^{-2} \cdot s^{-1}$). Culture mixing was achieved by gas bubbling in which CO_2 levels were maintained constant at 0.5% as in air-lift photobioreactors. Precise and constant level of CO_2 was supplied by a Gas Mixing System GMS 150 (Photon Systems Instruments, Czech Republic) following manufacturer's instructions. In a multicutivator system, growth was conducted in nutrient replete medium until day 3, then transferred to same medium without nitrogen to investigate possible impact on low nitrogen response. When needed, cells were counted using a LUNA Automated Cell Counter following manufacturer's instructions. For lipidomic analyses, cells were harvested by centrifugation at 3,500 × g for 10 minutes. Cells were then immediately frozen in liquid nitrogen and stored at -80°C, until use.

Design of vectors containing MgACSBG-specific TALE-N subunits

Transcription activator-like effector nucleases (TALE-N) consisted of restriction enzymes made of two subunits, called here Tal2Ng-R and Talg2Ng-L, engineered by fusing a TAL effector DNA-binding domain to a FokI DNA cleavage domain. The DNA binding domain contained a repeated highly conserved amino acid sequence with divergent amino acids, referred to as the repeat variable diresidue (RVD). The Tal2Ng-L and Tal2Ng-R RVDs were

purchased from ThermoFisher GeneArt-TALs and synthetized into their commercial vector. Tal2Ng-L subunit was designed following established guidelines (Sanjana et al., 2012) to bind to the TCCTGCGCATGGTGCCATT sequence in the *MgACSB* gene (Naga_100014g59), corresponding to RVD (T)-HD-HD-NG-NN-HD-NNHD-NI-NG-NN-NN-NG-NN-HD-HD-NI-NG-NG, whereas the Tal2Ng-R subunit was designed to bind specifically to TGGCAATGAGCCATTCGGG, corresponding to RVD (T)-NN-NN-HD-NI-NI-NGNN-NI-NN-HD-HD-NI-NG-NG-HD-NN-NN-NN. In these RVD sequences, '(T)' indicates that the first binding repeat is provided by the vector. Part of the Tal2Ng-L and Tal2Ng-R commercial sequences (comprising RVDs) were subcloned in two distinct home-designed vectors pCT5Ng and pCT6Ng to give pCT61 and pCT62, respectively. pCT5Ng is a pET15b backbone which contains a first part with the bleomycin/zeomycin-resistance protein from *Streptoalloteichus hindustanus* (ShBle) under the control of the UEP and with the fcpA terminator and a second part with a codon-adapted nuclear localization sequence (NLS) DYKDHDGDYKDHDIDYKDDDDKMAPKKKRKVGIHGVPAA (Sanjana et al., 2012), a codon-adapted HA-tag, N-ter sequence of commercial TAL up to *AflII* site, C-ter sequence of commercial TAL from *XhoI* site under the control of the endogenous ubiquitin extension promoter (UEP) and with the fcpA terminator. pCT6Ng is a pET28b backbone which contains a first part with the bleomycin/zeomycin-resistance protein from *Streptoalloteichus hindustanus* (ShBle) under the control of the UEP and with the fcpA terminator and a second part with a codon-adapted nuclear localization sequence (NLS) DYKDHDGDYKDHDIDYKDDDDKMAPKKKRKVGIHGVPAA (Sanjana et al., 2012), a codon-adapted HA-tag, N-ter sequence of commercial TAL up to *AflII* site, C-ter sequence of commercial TAL from *XhoI* site under the control of the endogenous ubiquitin extension promoter (UEP) and with the fcpA terminator. Codon optimization for expression in *M. gaditana* was done using the Kazusa webtool (http://www.kazusa.or.jp/codon/).

590 ***Nuclear transformation of* M. gaditana**

591 Plasmids pCT61 and pCT62 were linearized by digestion with ScaI and column-purified
592 using a NucleoSpin gel and polymerase chain reaction (PCR) clean-up kit (Macherey-Nagel)
593 following manufacturer's instructions. Two micrograms (one microgram TALE-N left subunit
594 plasmid + one microgram TALE-N right subunit plasmid) linearized plasmids were
595 electroporated into *M. gaditana* as previously described (Dolch et al., 2017). Transformed
596 lines were selected on f/2 plates containing 7 $\mu g.mL^{-1}$ zeocin. Integration of both TALE-N
597 subunits was assessed by colony PCR with primers TAL-Nterm-Rev
598 (GCAGGTCGCTAAAAGAATCG) and TAL-HA Fw (CCCCGACTACGCTAGCG) for
599 TALEN left subunit and TAL-Nterm-Rev (GCAGGTCGCTAAAAGAATCG) and TAL-His
600 Fw (CACCACCACCACCACAGC) for TALEN right subunit.

601 ***T7 endonuclease test and sequencing of TALE-N genetic targets***

602 Following *M. gaditana* co-transformation with pCT61 and pCT62 and selection on zeocin,
603 obtained clones harboring both TALE-N subunits were firstly analyzed by treatment with a
604 T7 endonuclease (T7E1, New England Biolabs) to cleave DNA at mismatched positions and
605 assess occurrence of genome editing at the target locus. To this aim, a genomic fragment of
606 around 396 bp in the *MgACSB* gene (Naga_100014g59), where the FokI activity region is
607 placed asymmetrically from the 5' and 3' ends, was PCR-amplified from positive colonies,
608 using a proofreading polymerase. After electrophoresis of amplified DNA on a 1% agarose
609 gel, bands corresponding to the desired products were purified and quantified. For each clone,
610 1.3 µg of PCR product was treated with T7E1 (+) or left untreated (-). A non-transformed
611 wild-type (WT) colony was also included as a negative control. T7E1 reaction was performed
612 following manufacturer's instruction, with the following minor modifications. One microliter
613 of T7E1 enzyme was used in each reaction and incubation performed at 37°C for one hour.
614 Separation of obtained fragments on 2% agarose gels allowed the detection of mismatched

615 DNA and occurrence of mutations at target sites in some of the clones tested. Positive *M.*
616 *gaditana* colonies were transferred onto a new selective plate to separate cells harboring the
617 mutation from those that presented a WT-like sequence. Mutation at *MgACSBG* target sites
618 was confirmed by sequencing of the DNA at the target locus (Eurofins, France).

619 ***Glycerolipid analyses***

620 Glycerolipids were extracted from freeze-dried *M. gaditana* cells grown in 50 mL of indicated
621 medium. About 50 to 100 × 10^6 cells were required for each triplicate analysis. A freeze-dried
622 pellet was suspended in 4 mL of boiling ethanol for 5 minutes to prevent lipid degradation,
623 and lipids were extracted as described earlier (Simionato et al., 2013) by addition of 2 mL
624 methanol and 8 mL chloroform at room temperature. The mixture was saturated with argon
625 and stirred for 1 hour at room temperature. After filtration through glass wool, cell debris was
626 rinsed with 3 mL chloroform/methanol 2:1, v/v, and 5 mL of NaCl 1%, w/v, was then added
627 to the filtrate to initiate biphase formation. The chloroform phase was collected and dried
628 under argon before solubilizing the lipid extract in 1 ml of chloroform. Total glycerolipids
629 were quantified based on their fatty acid (FA) content: in a 10 µl aliquot fraction, a known
630 quantity of 15:0 was added and FAs were converted into FA methyl esters (FAME) by a 1
631 hour incubation in 3 mL 2.5% H_2SO_4 in pure methanol, v/v, at 100°C (Jouhet et al., 2003).
632 The reaction was stopped by addition of 3 mL water, and 3 mL hexane was added for phase
633 separation. After 20 minutes incubation, the hexane phase was transferred to a new tube.
634 FAMEs were extracted a second time via the addition, incubation and extraction of another 3
635 mL hexane. The combined 6 mL were argon-dried and re-suspended in 30 µl hexane for gas
636 chromatography-flame ionization detector (GC-FID) (Perkin Elmer) analysis on a BPX70
637 (SGE) column. FAMEs were identified by comparison of their retention times with standards
638 (Sigma) and quantified by the surface peak method using 15:0 for calibration. Extraction and
639 quantification were performed with at least three biological replicates. Glycerolipids were

then analyzed and quantified by high pressure liquid chromatography-tandem mass spectrometry (HPLC-MS/MS), with appropriate standard lipids. The lipid extracts corresponding to 25 nmol of total fatty acids were dissolved in 100 µL of chloroform/methanol [2/1, (v/v)] containing 125 pmol of each internal standard. Internal standards used were phosphatidylethanolamine (PE) 18:0-18:0 and diacylglycerol (DAG) 18:0-22:6 from Avanti Polar Lipid, and sulfoquinovosyldiacylglycerol (SQDG) 16:0-18:0 extracted from spinach (*Spinacia oleracea*) thylakoid (Deme et al., 2014) and hydrogenated (Buseman et al., 2006). Lipids were then separated by HPLC and quantified by MS/MS. The HPLC separation method was adapted from previously described procedure (Rainteau et al., 2012). Lipid classes were separated using an Agilent 1200 HPLC system using a 150 mm × 3 mm (length × internal diameter) 5 µm diol column (Macherey-Nagel), at 40°C. The mobile phases consisted of hexane/isopropanol/water/1 M ammonium acetate, pH 5.3 [625/350/24/1, (v/v/v/v)] (A) and isopropanol/water/1 M ammonium acetate, pH 5.3 [850/149/1, (v/v/v)] (B). The injection volume was 20 µL. After 5 min, the percentage of B was increased linearly from 0% to 100% in 30 min and kept at 100% for 15 min. This elution sequence was followed by a return to 100% A in 5 min and an equilibration for 20 min with 100% A before the next injection, leading to a total runtime of 70 min. The flow rate of the mobile phase was 200 µL/min. The distinct glycerophospholipid classes were eluted successively as a function of the polar head group. Mass spectrometric analysis was performed on a 6460 triple quadrupole mass spectrometer (Agilent) equipped with a Jet stream electrospray ion source under following settings: drying gas heater at 260°C, drying gas flow at 13 $L \cdot min^{-1}$, sheath gas heater at 300°C, sheath gas flow at 11 $L \cdot min^{-1}$, nebulizer pressure at 25 psi, capillary voltage at ± 5000 V and nozzle voltage at ± 1,000 V. Nitrogen was used as collision gas. The quadrupoles Q1 and Q3 were operated at widest and unit resolution respectively. Phosphatidylcholine (PC) and diacylglyceryl-3-O-4'-(N,N,N-trimethyl)-homoserine (DGTS)

665 analyses were carried out in positive ion mode by scanning for precursors of m/z 184 and 236
666 respectively at a collision energy (CE) of 34 and 52 eV. SQDG analysis was carried out in
667 negative ion mode by scanning for precursors of m/z -225 at a CE of -56eV. PE,
668 phosphatidylinositol (PI), phosphatidylglycerol (PG), monogalactosyldiacylglycerol (MGDG)
669 and digalactosyldiacylglycerol (DGDG) measurements were performed in positive ion mode
670 by scanning for neutral losses of 141 Da, 277 Da, 189 Da, 179 Da and 341 Da at CEs of 20
671 eV, 12 eV, 16 eV, 8 eV and 8 eV, respectively. DAG and triacylglycerol (TAG) species were
672 identified and quantified by multiple reaction monitoring (MRM) as singly charged ions
673 $[M+NH4]^+$ at a CE of 16 and 22 eV respectively. Quantification was done for each lipid
674 species by multiple reaction monitoring (MRM) with 50 ms dwell time with the various
675 transitions previously recorded. Mass spectra were processed using the MassHunter
676 Workstation software (Agilent) for identification and quantification of lipids. Lipid amounts
677 (pmol) were corrected for response differences between internal standards and endogenous
678 lipids as described previously (Jouhet et al., 2017).

679 ***Acyl-CoA Analysis***

680 Freshly harvested cells cultivated in 10X ESAW (nutrient replete) medium were frozen in
681 liquid nitrogen, lyophilized and transferred to Rothamsted Research, UK for acyl-CoA
682 extraction and analysis (15 to 30 mg dry weight per sample). In brief, acyl-CoAs were
683 extracted using a bead beating method and analyzed using liquid chromatography coupled to
684 tandem mass spectrometry (LC-MS/MC) plus multireaction monitoring (MRM) in positive
685 ion mode. Acyl-CoA extraction efficiency was normalized to a 17:0 CoA (Sigma-Aldrich)
686 internal standard. All samples were immediately analyzed after extraction and were
687 maintained on a cooled stage prior to LC-MS/MS plus MRM analysis (using an ABSciex
688 4000 QTRAP device), as described earlier (Haynes et al., 2008) using an Agilent 1200 LC
689 system with a Agilent Eclipse XDB-C18 (3 × 100 mm; 3.5-µm particle size) column. For the

purposes of identification and calibration, standard acyl-CoA esters with acyl chain lengths from C10 to C20 (10:0; 12:0; 14:0; 16:0; 16:1; 16:3; 18:0; 18:1; 18:2; 18:3; 18:4; 18:5; 20:0; 20:3; 20:4; 20:5) were purchased from Sigma-Aldrich as free acids or lithium salts.

Modeling of MgACSBG structure bound to Coenzyme A, alpha-linolenic acid (18:3) and AMP

Structure modeling was based on the identification of acyl-CoA synthetase conserved motifs, secondary structure predictions and alignments with homologous sequences, for which protein 3D structures have been resolved and stored in the Protein Data Bank (PDB, (Burley et al., 2019)). Motif predictions were performed using the online servers MOTIF (Kanehisa et al., 2002), PROSITE (Sigrist et al., 2013) and Superfamily (Wilson et al., 2009). Secondary structures were predicted using the Porter (Mirabello and Pollastri, 2013) and Predictprotein (Yachdav et al., 2014) online tools. Search for homologous sequences was performed using Blast (Altschul et al., 1990). Automated structure prediction was attempted using Robetta (Song et al., 2013), RaptorX (Kallberg et al., 2012), Swiss-Model (Waterhouse et al., 2018), PhyRe2 (Kelley et al., 2015), I-Tasser (Zhang, 2009), PsiPred (Buchan et al., 2013) and PS(2) (Huang et al., 2015) servers. Four templates were selected for MgACSB modeling: 1ULT, (a long chain fatty acyl-CoA synthetase homodimer from *Thermus thermophiles*) (Hisanaga et al., 2004); 1PG4 (acetyl-CoA synthetase from *Salmonella enterica*) (Gulick et al., 2003); 5MSC (the A domain of carboxylic acid reductase from *Nocardia iowensis*) (Gahloth et al., 2017); 3EQ6, a human acyl-CoA synthetase medium-chain family member (Kochan et al., 2009). The sequences of these four template proteins were aligned with MgACSBG in Supplemental Fig. S4. 3D structural homology models were built with Modeller (Sali and Blundell, 1993) for the full length MgACSBG protein, from residue M1 to A649. Modeller being able to use multiple structure alignments, four models were built using different association of template proteins: M1pg4 from 1PG4 alone, M3eq6 from 3EQ6 alone and two consensus models Mcons1 from 1PG4, 1ULT and 5MSC and Mcons2 from all four protein

templates (Supplemental data 1 to 4). Positioning of CoA and AMP in the models was based on their neighboring residues in structures 1PG4 and 3EQ6 (Supplemental Tables S2A and S2B) using a transformation matrix to orient these residues in the X-ray structure of 1PG4 towards their homologs in the models of MgACSBG. In brief, to position CoA, backbone atoms of residues 305, 356, 357, 360, etc. in 1PG4 were translated and rotated to minimize the root-mean-square (rms) deviation with residues 259, 310, 311, 314, etc. in the model of MgACSBG. The same transformation was applied on the CoA molecule present in 1PG4 to properly insert it in the models. An AMP molecule, also present in 1PG4, was positioned in the two models M1pg4 and Mcons1, in the same way. Since 3EQ6 also contains both CoA and AMP, the positioning of CoA and AMP in models M3eq6 and Mcons2 was done using the matrix transformations pertaining to 3EQ6. As an example of a fatty acid, α-linolenic acid (18:3; $C_{18}H_{30}O_2$ *cis*-Δ9,12,15) was used. The lipid was initially placed manually inside the structures with the head in the direction of AMP, respecting its proximity with CoA and profiting of hydrophobic holes seen in the structures. The final models were finally energy minimized with the molecular dynamics program CHARMM (Brooks et al., 2009) using distance restraints between residues listed in Supplemental Table S2A and S2B and AMP or CoA. All missing parameters in the CHARMM force field were obtained from the SwissParam server (Zoete et al., 2011). All models were checked for allowed residues in the Ramachandran plot (Ramachandran et al., 1963) and corrected in case of presence of *D*-amino acids or *cis*-peptide bonds with Procheck (Laskowski et al., 1993). Finally, all models were subject to 1 ns Langevin molecular dynamic (MD) simulation at 300 K to regularize the structures before a final minimization. A summary of model energies and number of misplaced residues is shown in Supplemental Table S3. Three models M1pg4, M3eq6 and Mcons1, have similar final energy and correctly respect the restraints. Mcons2 shows a larger energy due mainly to the more difficult respect of distance restraints. All of them present in

regions distant from the active site, long unstructured loops and some amino acids in disallowed regions of the Ramachandran plot (Ramachandran et al., 1963). All models are provided as Supplemental data (model) 1 to 4.

Yeast expression of MgACSBG variants

Strains and growth media.

The isogenic *Saccharomyces cerevisiae* strains WT (YB332: MATa ura3 leu2 his3A200 ade2 lys2-801) and *faa1Δfaa4Δ* (YB525: MATa ura3 leu2 his3Δ200 ade2 lys2–801 faa1Δ::HIS3; faa4Δ::LYS2) used in this study were kindly provided by Dr. Paul Black (University of Nebraska at Lincoln, USA) and have been described earlier (Johnson et al., 1994; Johnson et al., 1994). After transformation, all the strains described in the present work were grown on synthetic media containing 6.7 $g.L^{-1}$ of Yeast Nitrogen Base (YNB, MP biomedicals), 0.77 $g.L^{-1}$ of CSM-URA (MP biomedicals) and $g.L^{-1}$ of either raffinose or galactose, as described. In complementation experiments, the media were supplemented with 22.5 µM cerulenin (Sigma-Aldrich), 100 µM free fatty acid (FFA) and 0.2% (v/v) final concentration TWEEN 80 (Sigma-Aldrich). The different FFAs were dissolved in 100% TWEEN 80 at a concentration of 50 mM. Cerulenin was dissolved in acetone at 45 mM. As controls, media without FFAs and/or cerulenin were also supplemented with 0.2% (v/v) TWEEN 80 and/or acetone.

Cloning of the coding sequences of variants of *MgACSBG*.

The three variants of *MgACSBG* (MgACSBG, MgACSBG#5 and MgACSBG#31) were cloned into the PstI-BamHI cloning site of the YEplac195 backbone (X75459.1) under the control of a galactose inducible promoter (pGAL1) and with the ADH1 terminator (t-ADH1). A 6× His tag was cloned in frame with the genes of interest in 3', upstream and in frame with the stop codon. Cloning was performed using the NEB Gibson Assembly Master Mix following manufacturer's instructions. Fragments of the pGAL1 promoter, the t-ADH1

terminator, and WT or mutated MgACSBG coding sequences were amplified by polymerase chain reaction (PCR) performed with Thermo Scientific Phusion High-Fidelity DNA Polymerase, following the manufacturer's instructions. The assembled plasmids were transformed in MAX Efficiency DH5α Competent Cells. Ampicillin resistant *Escherichia coli* colonies were PCR screened using pGAL1 and t-ADH1 flanking primers to validate the insert size. Two PCR positive colonies per construct were sequenced. The sequence-validated plasmids were transformed in the *faa1Δfaa4Δ Saccharomyces cerevisiae* double mutant by the Lithium acetate method (Gietz and Schiestl, 2007) and selected on CSM-Ura. As controls, WT and *faa1Δfaa4Δ* strains were transformed with the empty YEplac195 vector.

Three clones per transformation were used for complementation tests. For each experiment, one colony was inoculated in 2.7 mL of CSM-URA + raffinose and grown over-night at 30°C at 250 rpm. Transgene expression was induced by the addition of galactose 2% (p/v) final concentration and incubation for 6 hours before measurement of the optical density at 600 nm. Time course was performed in 96-well microplates (Thermo Scientific Nunc MicroWell 96-Well, Nunclon Delta-Treated, Flat-Bottom Microplate) filled with 200 µl of culture in galactose medium supplemented or not by FA or cerulenin and set at an OD_{600} = 0.3. The microplate was incubated at 30 ± 0.5°C in an Infinite M1000 PRO microplate reader (Tecan) set for plate orbital shake for 15 seconds every 20 minutes and absorbance measurements (OD_{600}) every 60 minutes, with four measurements per well. To the OD_{600} reads from experimental wells, the OD_{600} measured in blank wells containing the culture media only were subtracted to obtain adjusted OD_{600} values. Such values were transformed using an equation experimentally calculated from a calibration curve using an Eppendorf BioPhotometer UV/Vis Spectrophotometer.

Protein expression levels were evaluated by immunoblot analyses. After induction, an amount of cells corresponding to an OD_{600} of 50 was retrieved by a centrifugation of 3 minutes at 600

×g and washed with one milliliter of sterile water. Cells were resuspended in 200 µL of protein extraction buffer (150 mM Tris-HCl pH6.8, 8M urea, 1 mM EDTA, 1 mM DTT), and 100 µL of acid-washed 0.5 µm glass beads were added. Cells were heated for 5 minutes at 70°C and ground using the PreCellys Evolution (Bertin Instruments) by 3 cycles of 20 s of agitation at 10000 r.p.m. with pauses of 30 s between each cycle. The heating and grinding steps were performed twice and samples were centrifuged 5 minutes at 5000 ×g at 4°C. The supernatant was retrieved, and proteins were quantified using Bradford Assay (BioRad) according to manufacturer's instructions. Twenty micrograms of total proteins were used for immunoblot analysis. Proteins were separated on Bolt Bis-Tris Plus 4-12% (Life technologies) polyacrylamide gels in MES SDS Novex Bolt migration buffer (Life technologies) and then transferred in liquid in Novex Bolt Transfer buffer (Life technologies) according to manufacturer's instructions. Immunoblots were performed with anti-His C-Term antibodies (Invitrogen) to detect MgACSBG expression and anti-Kar2 antibodies (Santa Cruz Biotechnology) for loading control. Revelation was performed with Clarity Western Blot ECL substrate (BioRad) using an ImageQuant800 imager (Amersham).

Accession numbers

Naga_100014g59; Naga_100012g66; Naga_101051g1; Naga_100047g8; Naga_100649g1; Naga_100035g43; Phatr3_J20143; Phatr3_J12420; Phatr3_J54151; Phatr3_J45510; Phatr3_J17720; NP_524698; NP_001285923; NP_444408; XP_015155301; Q96GR2; Q5FVE4; F1NLD6.

Supplemental Data

Supplemental Figure S1. Overview of glycerolipid biosynthesis.

Supplemental Fig. S2. Multiple alignment of ACSBG proteins sequences from animals and heterokonts.

Supplemental Fig. S3. Secondary structure prediction of MgACSBG (Naga_100014g59).

Supplemental Fig. S4. Sequence Alignment of MgACSBG (Naga_100014g59 or NAGA) with proteins of known 3D-structure.

Supplemental Fig. S5. Expression of MgACSBG, MgACSBG#5 and MgACSBG#31 in the *S. cerevisiae faa1Δfaa4Δ* double mutant.

Supplemental Table S1. In depth analysis of phosphatidylcholine (PC) and betaine lipid (DGTS) fatty acid profiling by mass spectrometry.

Supplemental Table S2. Aminoacids in MgACSBG sequence predicted to be in the vicinity of Coenzyme A (CoA) and Adenosine monophosphate (AMP).

Supplemental Table S3. Evaluation of 3D-models of MgACSBG.

Supplemental Model 1. Model (1) acs4_3eq6_ac_3eq6_lipr_d1_min, in pdb format

Supplemental Model 2. Model (2) acs4_al2_ac_3eq6_lipr_d1_min, in pdb format

Supplemental Model 3. Model (3) acs4_all_ac_1pg4_lipr_min, in pdb format

Supplemental Model 4. Model (4) acs4_1pg4_ac_1pg4_lipr_min, in pdb format

Acknowledgements: This work was supported by the French National Research Agency (Oceanomics ANR-11-BTBR-0008, GRAL Labex ANR-10-LABEX-04, and EUR CBS ANR-17-EURE-0003) and by a CEA-Total partnership. Lipid analyses were performed at the LIPANG platform, with support from Conseil Régional Auvergne Rhône-Alpes, the European Commission and Institut Carnot 3BCAR. Authors are thankful to Richard Haslam for acyl-CoA analyses (Rothamsted Research, UK), Paul Black (University of Nebraska at Lincoln, USA) who kindly provided yeast strains, and Camille Rak, Clément Grant, Morgane Lapeyre, Valérie Gros, Melissa Conte, Julie Marais, Guillaume Tourcier and Christelle Richard for

837 technical assistance. Authors wish to express their sadness and gratitude to one of the
838 coauthors, Serge Crouzy, who unfortunately passed away in April 2020.

Figure Legends

Figure 1: Central role of acyl-CoAs in cell metabolism. (A) In this simplified scheme, acyl-CoAs are initially generated from fatty acids synthesized *de novo* by the action of specific ACSs. **(B)** Acyl-CoAs can be esterified to the *sn*-1 and *sn*-2 position of glycerol-3-phosphate, thus generating phosphatidic acid, which serves as a substrate for diacylglycerol and other membrane glycerolipids. Some specific acyl-CoAs, such as 18:3-CoA, can be further elongated and transferred to specific glycerolipids for additional desaturations (dashed lines), thus producing very-long chain polyunsaturated fatty acids (VLC-PUFAs). **(C)** Acyl-CoAs can be esterified to the *sn*-3 position of diacylglycerol to form triacylglycerol. **(D)** Furthermore, acyl-CoAs can be used for the synthesis of a variety of other acyl-molecules, such as sphingolipids, acylated proteins, sterol esters, and signaling molecules. **(E)** In this scheme, fatty acids hydrolyzed from membrane glycerolipids or triacylglycerol can re-enter the pool of acyl-CoAs by the action of other specific ACSs. **(F)** Eventually, Acyl-CoAs can be degraded via the beta-oxidation pathway occurring in mitochondria and/or peroxisomes. Adapted from (Coleman et al., 2002).

Figure 2. Motif conservation in Acyl-CoA synthetases of the Bubblegum family (ACSBGs) defined by Steinberg et al., 2000. Residues conserved in more than 50% of the sequences are shown in black boxes. This motif is based on a comprehensive comparison of ACS sequences in eukaryotes (Steinberg et al., 2000). Alignment includes sequences from fruit fly (*Drosophila melanogaster*; dmBG AAF44848 and dmBG-H1 AAF44850), mouse (*Mus musculus*; mmBG AA111606), human (*Homo sapiens*; HsACBG1 and HsACBG2), chicken (*Gallus gallus*, GgACSBG1 and GgACSBG2), *Michrochloropsis gaditana* (MgACSBG or Naga_100014g59) and *Phaedoctylum tricornutum* (Phatr3_J45510).

Figure 3: Phylogenetic comparison of acyl-CoA synthetases (ACS) from *M. gaditana* and *P. tricornutum*, with ACSBG sequences from Metazoa. All genes annotated as acyl-CoA synthetases or ligases from *M. gaditana* (Naga_100014g59, MgACSBG/Naga_100014g59; Naga_100012g66; Naga_101051g1; Naga_100047g8; Naga_100649g1 and Naga_100035g43) and *P. tricornutum* (Phatr3_J20143, ACS1; Phatr3_J12420, ACS2; Phatr3_J54151, ACS3; Phatr3_J45510, PtACSBG or ACS4; and Phatr3_J17720, ACL1) were compared with ACSBG sequences from *D. melanogaster* (DmACSBGa, NP_524698; DmACSBGc, NP_001285923); *H. sapiens* (HsACBG1, Q96GR; HsACBG2, Q5FVE4); *M. musculus* (MmACSBG1, NP_444408); *G. gallus* (GgACSBG1, F1NLD6; GgACSBG2, XP_015155301). The tree was calculated using a Bayesian inference method (MrBayes) as described in the Methods section, a Poisson model for amino acid substitutions, four Markov chain Monte Carlo (MCMC) chains run for 10,000 generations, sampling every 10 generations and a 50% majority rule consensus tree.

Figure 4: **MgACSBG mutants. (A)** Mutant selection. Following *M. gaditana* co-transformation with the two specifically designed TALE-N subunits, obtained clones were analyzed by treatment with a T7 endonuclease to detect cleaved DNA at mismatched positions and assess occurrence of genome editing at the target locus. When this test allowed detecting a mutation, the cell population was sub-cloned onto a new selective plate, and colonies arising from single cells were sequenced at the MgACSBG inside the FokI activity region (frame), resulting in the appearance of novel codons. Three mutant lines harboring mutated endogenous *MgACSBG* are shown, called here MgACSBG#5, MgACSBG#31 and MgACSBG#40. Only two to three aminoacids were modified in the endogenous proteins. **(B)** Point mutations in MgACSBG#5, MgACSBG#31 and MgACSBG#40. In grey boxes, wild type (WT) residues at the TALE-N nucleotidic target; in black boxes, inserted mutations.

Figure 5: Compared analysis of MgACSBG#5 and MgACSBG#31 with untransformed wild-type cells (WT) and cells transformed with an empty vector (EV). **(A)** Growth was measured by cell counting as described in the Methods section at days 3, 7 and 12 following inoculation (D3, D7 and D12, respectively). D3 corresponds to nutrient replete cultivation, whereas D7 and D12 correspond to nitrogen-starved condition. **(B)** Fatty acid content per million cells at D3, D7 and D12 following inoculation. **(C)** Triacylglycerol content, in mol% of total glycerolipids, at D3, D7 and D12 following inoculation. **(D)** Fatty acid profile at D3. Total FAs were extracted and, following methanolysis, obtained FA methyl esters were analyzed and quantified by gas chromatography coupled with ion flame detection (GC-FID), as described in the Methods section. **(E)** Glycerolipid profile at D3. Each glycerolipid class was analyzed by liquid chromatography coupled to tandem mass spectrometry (LC-MSMS) and quantified as described in the Methods section. DAG, diacylglycerol; DGDG, digalactosyldiacylglycerol; DGTS, diacylglyceryl-N,N,N-trimethylhomoserine; FA, fatty acid; MGDG, monogalactosyldiacylglycerol; PC, phosphatidylcholine; PE, phosphatidylethanolamine; PG, phosphatidylglycerol; PI, phosphatidylinositol; SQDG, sulfoquinovosyldiacylglycerol; TAG, triacylglycerol. Data are the average of 4 replicates. Error bars, standard deviation. (*), *P-value* < 0.05; student's t-test using WT as a reference.

Figure 6: Comparison of the acyl profiles of glycerolipid classes in MgACSBG#5, MgACSBG#31, untransformed wild-type cells (WT) and cells transformed with an empty vector (EV). (A) Phosphatidylcholine, PC. (B) Diacylglyceryl-N,N,N-trimethylhomoserine, DGTS. (C) Phosphatidylethanolamine, PE. (D) Phosphatidylglycerol, PG. (E) Sulfoquinovosyldiacylglycerol, SQDG. (F) Monogalactosyldiacylglycerol, MGDG. (G) Digalactosyldiacylglycerol, DGDG. (H) Triacylglycerol, TAG. Major molecular species corresponding to combined mass given in number of carbons and of double bonds are indicated, based on previous regioselective analysis of *M. gaditana* glycerolipids (Alboresi et al., 2016). Molecular species of which the proportion increases in the membrane lipids of MgACSBG#5 and MgACSBG#31 are shown in red, whereas those of which the proportion decreases are shown in green. Data are the average of 4 replicates and are given in mol%. Error bars, standard deviation. (*), P-value < 0.05; student's t-test using WT as a reference.

Figure 7: Model for ACSBG role in *M. gaditana*. The scheme shows the major fatty acids in major glycerolipid classes, i.e. PC, DGTS, PE and TAG in the ER, and MGDG in the plastid. Each membrane glycerolipid class is shown as a grey block. TAG is shown in a grey circle. **(A)** *De novo* synthesis of fatty acids (FAs) in the stroma of the plastid. The action of FA synthetase of type II (FAS II) leads to the production of 16:0-ACP, which can be desaturated by a palmitoyl ACP desaturase (PAD) into 16:1-ACP. These acyls can be exported to the cytosol, possibly as free fatty acids, through the four limiting membranes of the plastid. **(B)** ACSBG phenotype is consistent with a role in the production of 16:1-CoA. Unknown ACS isoforms (ACSx) catalyze the production of 16:0-CoA. **(C)** The 16:1 is incorporated at the sn-2 position of ER lipids via LPAT1 in *N. oceanica* (Nobusawa et al., 2017). Impairment of ACSBG alters this process. **(D)** The 16:0-CoA is elongated into 18:0-CoA by the action of D0-ELO isoforms, as a committing step in the 16:0-to-20:5 synthesis pathway (Dolch et al., 2017). **(E)** VLC-PUFA synthesis, starting with the 18:0-to-18:3 desaturation on PC by the stepwise action of an ERD9FAD, an ERD12FAD and an ERD6FAD. Since PC accumulates 18 precursors (18:1 and 18:2), we consider that the mutants are likely impaired downstream, at the level of 18:3 elongation, leading therefore to the positioning of ACSBG at the level of 18:3-CoA production, feeding the Δ6-ELO isoform producing 20:3-CoA. Downstream processes, i.e. 20:3-to-20:5 desaturations occurring on DGTS would be consistently impaired, with a decrease in the end-product, 20:5. **(F)** Some 20:3-to-20:5 desaturation processes occurring in DGTS operate also in PE. The slowing down

of 20:5 synthesis also occurs in PE. **(G)** As a result, following the mass action law, the slowing down occurring in the 16:0-to-20:5 pathway is expected to lead to an over-accumulation of 16:0-CoA. Excess 16:0-CoA can be stored as TAG, via the DGAT/Kennedy pathway. **(H)** An important assumption for this model is that a positive feedback is exerted on the plastid, exporting most its FAs, and explaining that the omega pathway is activated to provide sufficient 20:5 to plastid glycerolipids to compensate the lack of 16-carbon substrates. AAS, acyl-ACP synthetase; ACS, acyl-CoA synthetase; DGAT, diacylglycerol acyltransferase; DGTS, diacylglyceryl-N,N,N-trimethylhomoserine; FAD, fatty acid desaturase; MGDG, monogalactosyldiacylglycerol; PAD, palmitoyl ACP desaturase; PC, phosphatidylcholine; PE, phosphatidylethanolamine; TAG, triacylglycerol.

Figure 8: Comparison of the acyl-CoA profiles in MgACSBG#5, MgACSBG#31, untransformed wild-type cells (WT) and cells transformed with an empty vector (EV). Cells were cultivated in nutrient replete conditions as described in the Methods section (D3). Mass-spectrometry based analysis and data processing were performed by Rothamsted Research, UK. Data are the average of 2 replicates. Error bars, standard deviation. (*), P-value < 0.05; student's t-test using WT as a reference.

Figure 9. 3D model of MgACSBG bound to CoA, AMP and α-linolenic acid (18:3). Four models of MgACSBG were obtained based on similarity with acetyl- and acyl-CoA synthetase of known 3D structure, as described in the Methods section. The Mcons1 model of MgACSBG is shown with the visualization program VMD (Humphrey et al., 1996). The backbone of residues around AMP and CoA, listed in Supplemental Table S2A and S2B, are shown in licorice. The IGF triad is represented in pink (I96, G97, F98). The conserved Y216-K225 active site is shown in licorice mode. The position of IGF close to 18:3 is similar in all four MgACSBG models. Abbreviations: COA, Coenzyme A; AMP, adenosine monophosphate; LIP, α-linolenic acid.

Figure 10. Growth complementation of a yeast mutant defective in acyl-CoA activity by MgACSBG variants. (A) WT yeast strain growth curves in galactose medium (Cer-, green circles, positive control), with the addition of 22.5 µM cerulenin only (Cer+, grey circles, negative control), or with the addition of 22.5 µM cerulenin and 100 µM of the following free fatty acids, 14:0, 16:0, 18:0, 18:1, 18:2 and 18:3 (curves ranging from blue to red). **(B)** Growth curves of MgACSBG complemented *faa1Δfaa4Δ* double yeast mutant in galactose medium supplemented by 22.5 µM cerulenin and 100 µM of FA (curves ranging from blue to red). Medium with 22.5µM cerulenin but FA was used as a negative control (Cer+, grey circles). Average (+/- standard deviation) of biological (n = 3, independent clones) as well as technical (n = 3) replicates are presented. **(C)** and **(D)** Growth curves of the *faa1Δfaa4Δ* double mutant complemented with MgACSBG (green squares), MgACSBG#5 (blue squares), and MgACSBG#31 (purple squares) in presence of 22.5µM cerulenin and 100 µM 14:0 (C) or 16:0 (D). The *faa1Δfaa4Δ* double mutant without complementation was used as negative control and represented by grey circles. Average (+/- standard deviation) of biological (n = 3, independent clones) replicates are presented.

References

Abida H, Dolch LJ, Mei C, Villanova V, Conte M, Block MA, Finazzi G, Bastien O, Tirichine L, Bowler C, Rebeille F, Petroutsos D, Jouhet J, Marechal E (2015) Membrane glycerolipid remodeling triggered by nitrogen and phosphorus starvation in Phaeodactylum tricornutum. Plant Physiol **167:** 118-136

Abida H, Ruchaud S, Rios L, Humeau A, Probert I, De Vargas C, Bach S, Bowler C (2013) Bioprospecting marine plankton. Mar Drugs **11:** 4594-4611

Alboresi A, Perin G, Vitulo N, Diretto G, Block MA, Jouhet J, Meneghesso A, Valle G, Giuliano G, Marechal E, Morosinotto T (2016) Light Remodels Lipid Biosynthesis in Nannochloropsis gaditana by Modulating Carbon Partitioning Between Organelles. Plant Physiol

Altschul SF, Gish W, Miller W, Myers EW, Lipman DJ (1990) Basic Local Alignment Search Tool. Journal of Molecular Biology **215:** 403-410

Bates PD, Fatihi A, Snapp AR, Carlsson AS, Browse J, Lu C (2012) Acyl editing and headgroup exchange are the major mechanisms that direct polyunsaturated fatty acid flux into triacylglycerols. Plant Physiol **160:** 1530-1539

Benning C (2008) A role for lipid trafficking in chloroplast biogenesis. Progress in Lipid Research **47:** 381-389

Benning C (2009) Mechanisms of lipid transport involved in organelle biogenesis in plant cells. Annu Rev Cell Dev Biol **25:** 71-91

Black PN, DiRusso CC (2007) Yeast acyl-CoA synthetases at the crossroads of fatty acid metabolism and regulation. Biochimica Et Biophysica Acta-Molecular and Cell Biology of Lipids **1771:** 286-298

Black PN, Zhang Q, Weimar JD, DiRusso CC (1997) Mutational analysis of a fatty acyl-coenzyme A synthetase signature motif identifies seven amino acid residues that modulate fatty acid substrate specificity. J Biol Chem **272:** 4896-4903

Botte CY, Yamaryo-Botte Y, Janouskovec J, Rupasinghe T, Keeling PJ, Crellin P, Coppel RL, Marechal E, McConville MJ, McFadden GI (2011) Identification of plant-like galactolipids in Chromera velia, a photosynthetic relative of malaria parasites. J Biol Chem **286:** 29893-29903

Boudiere L, Botte CY, Saidani N, Lajoie M, Marion J, Brehelin L, Yamaryo-Botte Y, Satiat-Jeunemaitre B, Breton C, Girard-Egrot A, Bastien O, Jouhet J, Falconet D, Block MA, Marechal E (2012) Galvestine-1, a novel chemical probe for the study of the glycerolipid homeostasis system in plant cells. Mol Biosyst **8:** 2023-2035, 2014

Boudiere L, Michaud M, Petroutsos D, Rebeille F, Falconet D, Bastien O, Roy S, Finazzi G, Rolland N, Jouhet J, Block MA, Marechal E (2014) Glycerolipids in photosynthesis: composition, synthesis and trafficking. Biochim Biophys Acta **1837:** 470-480

Brooks BR, Brooks CL, 3rd, Mackerell AD, Jr., Nilsson L, Petrella RJ, Roux B, Won Y, Archontis G, Bartels C, Boresch S, Caflisch A, Caves L, Cui Q, Dinner AR, Feig M, Fischer S, Gao J, Hodoscek M, Im W, Kuczera K, Lazaridis T, Ma J, Ovchinnikov V, Paci E, Pastor RW, Post CB, Pu JZ, Schaefer M, Tidor B, Venable RM, Woodcock HL, Wu X, Yang W, York DM, Karplus M (2009) CHARMM: the biomolecular simulation program. J Comput Chem **30:** 1545-1614

Buchan DW, Minneci F, Nugent TC, Bryson K, Jones DT (2013) Scalable web services for the PSIPRED Protein Analysis Workbench. Nucleic Acids Res **41:** W349-357

Burley SK, Berman HM, Bhikadiya C, Bi CX, Chen L, Di Costanzo L, Christie C, Duarte JM, Dutta S, Feng ZK, Ghosh S, Goodsell DS, Green RK, Guranovic V, Guzenko D, Hudson BP, Liang YH, Lowe R, Peisach E, Periskova I, Randle C, Rose A, Sekharan M, Shao CH, Tao YP, Valasatava Y, Voigt M, Westbrook J, Young J, Zardecki C, Zhuravleva M, Kurisu G, Nakamura H, Kengaku Y, Cho H, Sato J, Kim JY, Ikegawa Y, Nakagawa A, Yamashita R, Kudou T, Bekker GJ, Suzuki H, Iwata T, Yokochi M, Kobayashi N, Fujiwara T, Velankar S, Kleywegt GJ, Anyango S, Armstrong DR, Berrisford JM, Conroy MJ, Dana JM, Deshpande M, Gane P, Gaborova R, Gupta D, Gutmanas A, Koca J, Mak L, Mir S, Mukhopadhyay A, Nadzirin N, Nair S, Patwardhan A, Paysan-Lafosse T, Pravda L, Salih O, Sehnal D, Varadi M, Varekova R, Markley JL, Hoch JC, Romero PR, Baskaran K, Maziuk D, Ulrich EL, Wedell JR, Yao HY, Livny M, Ioannidis YE, Consortium W, Japan PDB (2019) Protein Data Bank: the single global archive for 3D macromolecular structure data. Nucleic Acids Research **47:** D520-D528

Buseman CM, Tamura P, Sparks AA, Baughman EJ, Maatta S, Zhao J, Roth MR, Esch SW, Shah J, Williams TD, Welti R (2006) Wounding stimulates the accumulation of glycerolipids containing oxophytodienoic acid and dinor-oxophytodienoic acid in Arabidopsis leaves. Plant Physiol **142:** 28-39

Camacho-Rodriguez J, Ceron-Garcia MC, Fernandez-Sevilla JM, Molina-Grima E (2015) Genetic algorithm for the medium optimization of the microalga Nannochloropsis gaditana cultured to aquaculture. Bioresour Technol **177:** 102-109

Camacho-Rodriguez J, Ceron-Garcia MC, Gonzalez-Lopez CV, Fernandez-Sevilla JM, Contreras-Gomez A, Molina-Grima E (2013) A low-cost culture medium for the production of Nannochloropsis gaditana biomass optimized for aquaculture. Bioresour Technol **144:** 57-66

Camacho-Rodriguez J, Gonzalez-Cespedes AM, Ceron-Garcia MC, Fernandez-Sevilla JM, Acien-Fernandez FG, Molina-Grima E (2014) A quantitative study of eicosapentaenoic acid (EPA) production by Nannochloropsis gaditana for aquaculture as a function of dilution rate, temperature and average irradiance. Appl Microbiol Biotechnol **98:** 2429-2440

Castresana J (2000) Selection of conserved blocks from multiple alignments for their use in phylogenetic analysis. Mol Biol Evol **17:** 540-552

Cavalier-Smith T (2018) Kingdom Chromista and its eight phyla: a new synthesis emphasising periplastid protein targeting, cytoskeletal and periplastid evolution, and ancient divergences. Protoplasma **255:** 297-357

Chen CY, Chen YC, Huang HC, Huang CC, Lee WL, Chang JS (2013) Engineering strategies for enhancing the production of eicosapentaenoic acid (EPA) from an isolated microalga Nannochloropsis oceanica CY2. Bioresour Technol **147:** 160-167

Claire D'Andre H, Paul W, Shen X, Jia X, Zhang R, Sun L, Zhang X (2013) Identification and characterization of genes that control fat deposition in chickens. J Anim Sci Biotechnol **4:** 43

Coleman RA, Lewin TM, Van Horn CG, Gonzalez-Baro MR (2002) Do long-chain acyl-CoA synthetases regulate fatty acid entry into synthetic versus degradative pathways? J Nutr **132:** 2123-2126

Degraeve-Guilbault C, Brehelin C, Haslam R, Sayanova O, Marie-Luce G, Jouhet J, Corellou F (2017) Glycerolipid Characterization and Nutrient Deprivation-Associated Changes in the Green Picoalga Ostreococcus tauri. Plant Physiol **173:** 2060-2080

Deme B, Cataye C, Block MA, Marechal E, Jouhet J (2014) Contribution of galactoglycerolipids to the 3-dimensional architecture of thylakoids. FASEB J **28:** 3373-3383

Dereeper A, Guignon V, Blanc G, Audic S, Buffet S, Chevenet F, Dufayard JF, Guindon S, Lefort V, Lescot M, Claverie JM, Gascuel O (2008) Phylogeny.fr: robust phylogenetic analysis for the non-specialist. Nucleic Acids Res **36:** W465-469

Dolch LJ, Lupette J, Tourcier G, Bedhomme M, Collin S, Magneschi L, Conte M, Seddiki K, Richard C, Corre E, Fourage L, Laeuffer F, Richards R, Reith M, Rebeille F, Jouhet J, McGinn P, Marechal E (2017) Nitric Oxide Mediates Nitrite-Sensing and Acclimation and Triggers a Remodeling of Lipids. Plant Physiol **175:** 1407-1423

Dolch LJ, Marechal E (2015) Inventory of fatty acid desaturases in the pennate diatom Phaeodactylum tricornutum. Mar Drugs **13:** 1317-1339

Dolch LJ, Rak C, Perin G, Tourcier G, Broughton R, Leterrier M, Morosinotto T, Tellier F, Faure JD, Falconet D, Jouhet J, Sayanova O, Beaudoin F, Marechal E (2017) A Palmitic Acid Elongase Affects Eicosapentaenoic Acid and Plastidial Monogalactosyldiacylglycerol Levels in Nannochloropsis. Plant Physiol **173:** 742-759

Edgar RC (2004) MUSCLE: multiple sequence alignment with high accuracy and high throughput. Nucleic Acids Res **32:** 1792-1797

Faergeman NJ, Black PN, Zhao XD, Knudsen J, DiRusso CC (2001) The acyl-CoA synthetases encoded within FAA1 and FAA4 in Saccharomyces cerevisiae function as components of the fatty acid transport system linking import, activation, and intracellular utilization. Journal of Biological Chemistry **276:** 37051-37059

Fawley MW, Jameson I, Fawley KP (2015) The phylogeny of the genus Nannochloropsis (Monodopsidaceae, Eustigmatophyceae), with descriptions of N. australis sp. nov. and Microchloropsis gen. nov. Phycologia **54:** 545-552

Flori S, Jouneau P-H, Finazzi G, Maréchal E, Falconet D (2016) Ultrastructure of the Periplastidial Compartment of the Diatom Phaeodactylum tricornutum. Protist **167:** 254-267

Fussy Z, Obornik M (2018) Complex Endosymbioses I: From Primary to Complex Plastids, Multiple Independent Events. Methods Mol Biol **1829:** 17-35

Gahloth D, Dunstan MS, Quaglia D, Klumbys E, Lockhart-Cairns MP, Hill AM, Derrington SR, Scrutton NS, Turner NJ, Leys D (2017) Structures of carboxylic acid reductase reveal domain dynamics underlying catalysis. Nat Chem Biol **13:** 975-981

Gietz RD, Schiestl RH (2007) Large-scale high-efficiency yeast transformation using the LiAc/SS carrier DNA/PEG method. Nature Protocols **2:** 38-41

Gulick AM, Starai VJ, Horswill AR, Homick KM, Escalante-Semerena JC (2003) The 1.75 A crystal structure of acetyl-CoA synthetase bound to adenosine-5'-propylphosphate and coenzyme A. Biochemistry **42:** 2866-2873

Haynes CA, Allegood JC, Sims K, Wang EW, Sullards MC, Merrill AH, Jr. (2008) Quantitation of fatty acyl-coenzyme As in mammalian cells by liquid chromatography-electrospray ionization tandem mass spectrometry. J Lipid Res **49:** 1113-1125

Hisanaga Y, Ago H, Nakagawa N, Hamada K, Ida K, Yamamoto M, Hori T, Arii Y, Sugahara M, Kuramitsu S, Yokoyama S, Miyano M (2004) Structural basis of the substrate-specific two-step catalysis of long chain fatty acyl-CoA synthetase dimer. J Biol Chem **279:** 31717-31726

Horn PJ, Benning C (2016) The plant lipidome in human and environmental health. Science **353:** 1228-1232

Huang TT, Hwang JK, Chen CH, Chu CS, Lee CW, Chen CC (2015) (PS)2: protein structure prediction server version 3.0. Nucleic Acids Res **43:** W338-342

Huelsenbeck JP, Ronquist F (2001) MRBAYES: Bayesian inference of phylogenetic trees. Bioinformatics **17:** 754-755

Humphrey W, Dalke A, Schulten K (1996) VMD: visual molecular dynamics. J Mol Graph **14:** 33-38, 27-38

Hurlock AK, Wang K, Takeuchi T, Horn PJ, Benning C (2018) In vivo lipid 'tag and track' approach shows acyl editing of plastid lipids and chloroplast import of phosphatidylglycerol precursors in Arabidopsis thaliana. Plant J **95:** 1129-1139

Iwai M, Hori K, Sasaki-Sekimoto Y, Shimojima M, Ohta H (2015) Manipulation of oil synthesis in Nannochloropsis strain NIES-2145 with a phosphorus starvation-inducible promoter from Chlamydomonas reinhardtii. Front Microbiol **6:** 912

Johnson DR, Knoll LJ, Levin DE, Gordon JI (1994) Saccharomyces cerevisiae contains four fatty acid activation (FAA) genes: an assessment of their role in regulating protein N-myristoylation and cellular lipid metabolism. J Cell Biol **127:** 751-762

Johnson DR, Knoll LJ, Rowley N, Gordon JI (1994) Genetic analysis of the role of Saccharomyces cerevisiae acyl-CoA synthetase genes in regulating protein N-myristoylation. J Biol Chem **269:** 18037-18046

Jouhet J, Lupette J, Clerc O, Magneschi L, Bedhomme M, Collin S, Roy S, Maréchal E, Rébeillé F (2017) LC-MS/MS versus TLC plus GC methods: Consistency of glycerolipid and fatty acid profiles in microalgae and higher plant cells and effect of a nitrogen starvation. PLOS ONE **12:** e0182423

Jouhet J, Marechal E, Bligny R, Joyard J, Block MA (2003) Transient increase of phosphatidylcholine in plant cells in response to phosphate deprivation. FEBS Lett **544:** 63-68

Kallberg M, Wang HP, Wang S, Peng J, Wang ZY, Lu H, Xu JB (2012) Template-based protein structure modeling using the RaptorX web server. Nature Protocols **7:** 1511-1522

Kanehisa M, Goto S, Kawashima S, Nakaya A (2002) The KEGG databases at GenomeNet. Nucleic Acids Res **30:** 42-46

Kang NK, Jeon S, Kwon S, Koh HG, Shin SE, Lee B, Choi GG, Yang JW, Jeong BR, Chang YK (2015) Effects of overexpression of a bHLH transcription factor on biomass and lipid production in Nannochloropsis salina. Biotechnol Biofuels **8:** 200

Kelley LA, Mezulis S, Yates CM, Wass MN, Sternberg MJ (2015) The Phyre2 web portal for protein modeling, prediction and analysis. Nat Protoc **10:** 845-858

Kochan G, Pilka ES, von Delft F, Oppermann U, Yue WW (2009) Structural Snapshots for the Conformation-dependent Catalysis by Human Medium-chain Acyl-coenzyme A Synthetase ACSM2A. Journal of Molecular Biology **388:** 997-1008

LaBrant E, Barnes AC, Roston RL (2018) Lipid transport required to make lipids of photosynthetic membranes. Photosynth Res **138:** 345-360

Laskowski RA, Macarthur MW, Moss DS, Thornton JM (1993) Procheck - a Program to Check the Stereochemical Quality of Protein Structures. Journal of Applied Crystallography **26:** 283-291

Li-Beisson Y, Neunzig J, Lee Y, Philippar K (2017) Plant membrane-protein mediated intracellular traffic of fatty acids and acyl lipids. Curr Opin Plant Biol **40:** 138-146

Li-Beisson Y, Shorrosh B, Beisson F, Andersson MX, Arondel V, Bates PD, Baud S, Bird D, Debono A, Durrett TP, Franke RB, Graham IA, Katayama K, Kelly AA, Larson T, Markham JE, Miquel M, Molina I, Nishida I, Rowland O, Samuels L, Schmid KM, Wada H, Welti R, Xu C, Zallot R, Ohlrogge J (2010) Acyl-lipid metabolism. *In* The Arabidopsis Book, Ed 2010/01/01 Vol 8, p e0133

Li-Beisson Y, Thelen JJ, Fedosejevs E, Harwood JL (2019) The lipid biochemistry of eukaryotic algae. Prog Lipid Res **74:** 31-68

Li N, Gugel IL, Giavalisco P, Zeisler V, Schreiber L, Soll J, Philippar K (2015) FAX1, a novel membrane protein mediating plastid fatty acid export. PLoS Biol **13:** e1002053

Li N, Xu C, Li-Beisson Y, Philippar K (2016) Fatty Acid and Lipid Transport in Plant Cells. Trends Plant Sci **21:** 145-158

Lopes-Marques M, Machado AM, Ruivo R, Fonseca E, Carvalho E, Castro LFC (2018) Expansion, retention and loss in the Acyl-CoA synthetase "Bubblegum" (Acsbg) gene family in vertebrate history. Gene **664:** 111-118

Lupette J, Jaussaud A, Seddiki K, Morabito C, Brugiere S, Schaller H, Kuntz M, Putaux JL, Jouneau PH, Rebellle F, Falconet D, Coute Y, Jouhet J, Tardif M, Salvaing J, Marechal E (2019) The architecture of lipid droplets in the diatom Phaeodactylum tricornutum. Algal Research-Biomass Biofuels and Bioproducts **38**

Ma AC, Chen Y, Blackburn PR, Ekker SC (2016) TALEN-Mediated Mutagenesis and Genome Editing. Methods Mol Biol **1451:** 17-30

Ma Y, Wang Z, Yu C, Yin Y, Zhou G (2014) Evaluation of the potential of 9 Nannochloropsis strains for biodiesel production. Bioresour Technol **167:** 503-509

Malzahn A, Lowder L, Qi Y (2017) Plant genome editing with TALEN and CRISPR. Cell Biosci **7:** 21

Mashek DG, Li LO, Coleman RA (2007) Long-chain acyl-CoA synthetases and fatty acid channeling. Future Lipidol **2:** 465-476

Mashek DG, McKenzie MA, Van Horn CG, Coleman RA (2006) Rat long chain acyl-CoA synthetase 5 increases fatty acid uptake and partitioning to cellular triacylglycerol in McArdle-RH7777 cells. J Biol Chem **281:** 945-950

Menard GN, Bryant FM, Kelly AA, Craddock CP, Lavagi I, Hassani-Pak K, Kurup S, Eastmond PJ (2018) Natural variation in acyl editing is a determinant of seed storage oil composition. Sci Rep **8:** 17346

Meng Y, Jiang J, Wang H, Cao X, Xue S, Yang Q, Wang W (2015) The characteristics of TAG and EPA accumulation in Nannochloropsis oceanica IMET1 under different nitrogen supply regimes. Bioresour Technol **179:** 483-489

Min KT, Benzer S (1999) Preventing neurodegeneration in the Drosophila mutant bubblegum. Science **284:** 1985-1988

Mirabello C, Pollastri G (2013) Porter, PaleAle 4.0: high-accuracy prediction of protein secondary structure and relative solvent accessibility. Bioinformatics **29:** 2056-2058

Moriya-Sato A, Hida A, Inagawa-Ogashiwa M, Wada MR, Sugiyama K, Shimizu J, Yabuki T, Seyama Y, Hashimoto N (2000) Novel acyl-CoA synthetase in adrenoleukodystrophy target tissues. Biochem Biophys Res Commun **279:** 62-68

Murakami H, Nobusawa T, Hori K, Shimojima M, Ohta H (2018) Betaine Lipid Is Crucial for Adapting to Low Temperature and Phosphate Deficiency in Nannochloropsis. Plant Physiol **177:** 181-193

Nobusawa T, Hori K, Mori H, Kurokawa K, Ohta H (2017) Differently localized lysophosphatidic acid acyltransferases crucial for triacylglycerol biosynthesis in the oleaginous alga Nannochloropsis. Plant J **90:** 547-559

Pei Z, Oey NA, Zuidervaart MM, Jia Z, Li Y, Steinberg SJ, Smith KD, Watkins PA (2003) The acyl-CoA synthetase "bubblegum" (lipidosin): further characterization and role in neuronal fatty acid beta-oxidation. J Biol Chem **278:** 47070-47078

Petroutsos D, Amiar S, Abida H, Dolch LJ, Bastien O, Rebeille F, Jouhet J, Falconet D, Block MA, McFadden GI, Bowler C, Botte C, Marechal E (2014) Evolution of galactoglycerolipid biosynthetic pathways--from cyanobacteria to primary plastids and from primary to secondary plastids. Prog Lipid Res **54:** 68-85

Poliner E, Farre EM, Benning C (2018) Advanced genetic tools enable synthetic biology in the oleaginous microalgae Nannochloropsis sp. Plant Cell Rep **37:** 1383-1399

Radakovits R, Jinkerson RE, Fuerstenberg SI, Tae H, Settlage RE, Boore JL, Posewitz MC (2012) Draft genome sequence and genetic transformation of the oleaginous alga Nannochloropis gaditana. Nat Commun **3:** 686

Rainteau D, Humbert L, Delage E, Vergnolle C, Cantrel C, Maubert MA, Lanfranchi S, Maldiney R, Collin S, Wolf C, Zachowski A, Ruelland E (2012) Acyl chains of phospholipase D transphosphatidylation products in Arabidopsis cells: a study using multiple reaction monitoring mass spectrometry. PLoS One **7:** e41985

Ramachandran GN, Ramakrishnan C, Sasisekharan V (1963) Stereochemistry of polypeptide chain configurations. J Mol Biol **7:** 95-99

Ronquist F, Teslenko M, van der Mark P, Ayres DL, Darling A, Hohna S, Larget B, Liu L, Suchard MA, Huelsenbeck JP (2012) MrBayes 3.2: efficient Bayesian phylogenetic inference and model choice across a large model space. Syst Biol **61:** 539-542

Sali A, Blundell TL (1993) Comparative protein modelling by satisfaction of spatial restraints. J Mol Biol **234:** 779-815

Sanjana NE, Cong L, Zhou Y, Cunniff MM, Feng G, Zhang F (2012) A transcription activator-like effector toolbox for genome engineering. Nat Protoc **7:** 171-192

Sayanova O, Mimouni V, Ulmann L, Morant-Manceau A, Pasquet V, Schoefs B, Napier JA (2017) Modulation of lipid biosynthesis by stress in diatoms. Philos Trans R Soc Lond B Biol Sci **372**

Sigrist CJ, de Castro E, Cerutti L, Cuche BA, Hulo N, Bridge A, Bougueleret L, Xenarios I (2013) New and continuing developments at PROSITE. Nucleic Acids Res **41:** D344-347

Simionato D, Block MA, La Rocca N, Jouhet J, Marechal E, Finazzi G, Morosinotto T (2013) The response of Nannochloropsis gaditana to nitrogen starvation includes de novo biosynthesis of triacylglycerols, a decrease of chloroplast galactolipids, and reorganization of the photosynthetic apparatus. Eukaryot Cell **12:** 665-676

Song SY, Kato C, Adachi E, Moriya-Sato A, Inagawa-Ogashiwa M, Umeda R, Hashimoto N (2007) Expression of an acyl-CoA synthetase, lipidosin, in astrocytes of the murine brain and its up-regulation during remyelination following cuprizone-induced demyelination. J Neurosci Res **85:** 3586-3597

Song YF, DiMaio F, Wang RYR, Kim D, Miles C, Brunette TJ, Thompson J, Baker D (2013) High-Resolution Comparative Modeling with RosettaCM. Structure **21:** 1735-1742

Steinberg SJ, Morgenthaler J, Heinzer AK, Smith KD, Watkins PA (2000) Very long-chain acyl-CoA synthetases. Human "bubblegum" represents a new family of proteins capable of activating very long-chain fatty acids. J Biol Chem **275:** 35162-35169

Van Vooren G, Le Grand F, Legrand J, Cuine S, Peltier G, Pruvost J (2012) Investigation of fatty acids accumulation in Nannochloropsis oculata for biodiesel application. Bioresour Technol **124:** 421-432

Vieler A, Wu G, Tsai CH, Bullard B, Cornish AJ, Harvey C, Reca IB, Thornburg C, Achawanantakun R, Buehl CJ, Campbell MS, Cavalier D, Childs KL, Clark TJ, Deshpande R, Erickson E, Armenia Ferguson A, Handee W, Kong Q, Li X, Liu B, Lundback S, Peng C, Roston RL, Sanjaya, Simpson JP, Terbush A, Warakanont J, Zauner S, Farre EM, Hegg EL, Jiang N, Kuo MH, Lu Y, Niyogi KK, Ohlrogge J, Osteryoung KW, Shachar-Hill Y, Sears BB, Sun Y, Takahashi H, Yandell M, Shiu SH, Benning C (2012) Genome, functional gene annotation, and nuclear transformation of the heterokont oleaginous alga Nannochloropsis oceanica CCMP1779. PLoS Genet **8:** e1003064

Waterhouse A, Bertoni M, Bienert S, Studer G, Tauriello G, Gumienny R, Heer FT, de Beer TAP, Rempfer C, Bordoli L, Lepore R, Schwede T (2018) SWISS-MODEL: homology modelling of protein structures and complexes. Nucleic Acids Res **46:** W296-W303

Watkins PA, Maiguel D, Jia Z, Pevsner J (2007) Evidence for 26 distinct acyl-coenzyme A synthetase genes in the human genome. J Lipid Res **48:** 2736-2750

Wilson D, Pethica R, Zhou YD, Talbot C, Vogel C, Madera M, Chothia C, Gough J (2009) SUPERFAMILY-sophisticated comparative genomics, data mining, visualization and phylogeny. Nucleic Acids Research **37:** D380-D386

Yachdav G, Kloppmann E, Kajan L, Hecht M, Goldberg T, Hamp T, Honigschmid P, Schafferhans A, Roos M, Bernhofer M, Richter L, Ashkenazy H, Punta M, Schlessinger A, Bromberg Y, Schneider R, Vriend G, Sander C, Ben-Tal N, Rost B (2014) PredictProtein--an open resource for online prediction of protein structural and functional features. Nucleic Acids Res **42:** W337-343

Zhang Y (2009) I-TASSER: fully automated protein structure prediction in CASP8. Proteins **77 Suppl 9:** 100-113

Zoete V, Cuendet MA, Grosdidier A, Michielin O (2011) SwissParam: a fast force field generation tool for small organic molecules. J Comput Chem **32:** 2359-2368

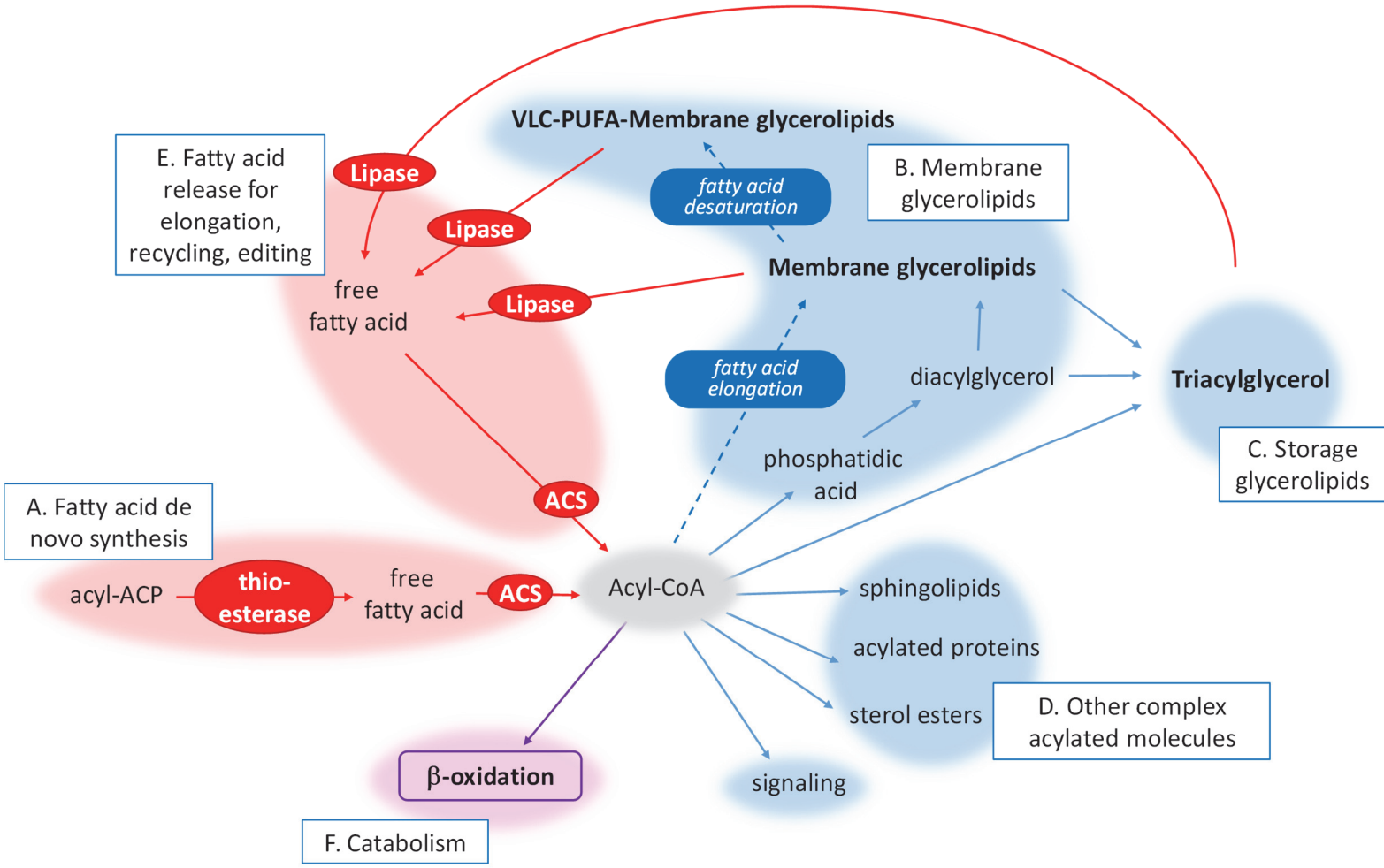

Figure 1: Central role of acyl-CoAs in cell metabolism. (A) In this simplified scheme, acyl-CoAs are initially generated from fatty acids synthesized *de novo*, by the action of specific ACSs. **(B)** Acyl-CoAs can be esterified to the *sn*-1 and *sn*-2 position of glycerol-3-phosphate, thus generating phosphatidic acid, which serves as a substrate for diacylglycerol and other membrane glycerolipids. Some specific acyl-CoAs, such as 18:3-CoA can be further elongated and transferred to specific glycerolipids for additional desaturations (dashed lines), thus producing very-long chain polyunsaturated fatty acids (VLC-PUFAs). **(C)** Acyl-CoAs can be esterified to the *sn*-3 position of diacylglycerol to form triacylglycerol. **(D)** Furthermore, acyl-CoAs can be used for the synthesis of a variety of other acyl-molecules, such as sphingolipids, acylated proteins, sterol esters, signaling molecules. **(E)** In this scheme, fatty acids hydrolyzed from membrane glycerolipids or triacylglycerol can re-enter the pool of acyl-CoAs by the action of other specific ACSs. **(F)** Eventually, Acyl-CoAs can be degraded via the beta-oxidation pathway occurring in mitochondria and/or peroxisomes. Adapted from (Coleman et al., 2002).

Figure 2. Motif conservation in Acyl-CoA synthetases of the Bubblegum family (ACSBGs) defined by Steinberg et al., 2000. Residues conserved in more than 50% of the sequences are shown in black boxes. This motif is based on a comprehensive comparison of ACS sequences in eukaryotes (Steinberg et al., 2000).

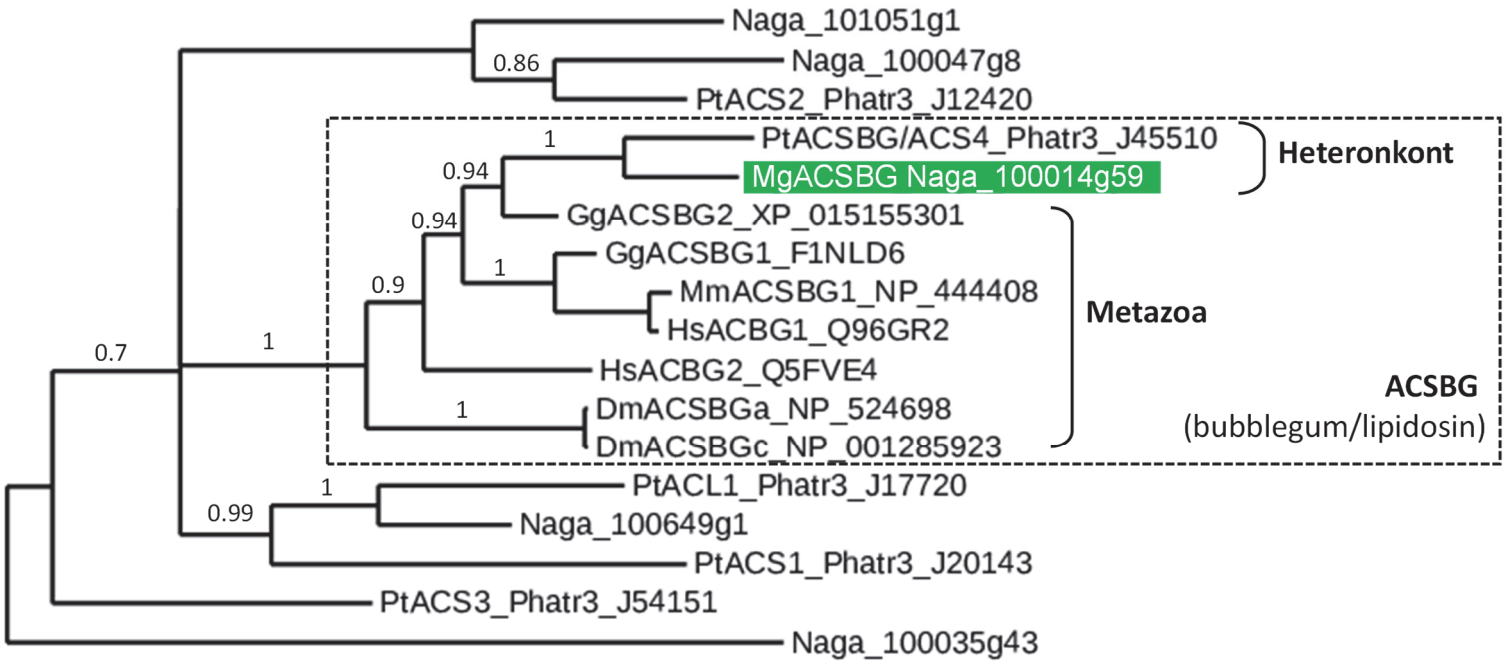

Figure 3: Phylogenetic comparison of acyl-CoA synthetases (ACS) from *M. gaditana* and *P. tricornutum*, with ACSBG sequences from Metazoa. All genes annotated as acyl-CoA synthetases or ligases from M. gaditana (Naga_100014g59, MgACSBG/Naga_100014g59; Naga_100012g66; Naga_101051g1; Naga_100047g8; Naga_100649g1 and Naga_100035g43) and P. tricornutum (Phatr3_J20143, ACS1; Phatr3_J12420, ACS2; Phatr3_J54151, ACS3; Phatr3_J45510, PtACSBG or ACS4; and Phatr3_J17720, ACL1) were compared with ACSBG sequences from D. melanogaster (DmACSBGa, NP_524698; DmACSBGc, NP_001285923); H. sapiens (HsACBG1, Q96GR; HsACBG2, Q5FVE4); M. musculus (MmACSBG1, NP_444408); G. gallus (GgACSBG1, F1NLD6; GgACSBG2, XP_015155301). The tree was calculated using a Bayesian inference method (MrBayes) as described in the Method section, a Poisson model for amino acid substitutions, four Markov chain Monte Carlo (MCMC) chains run for 10,000 generations, sampling every 10 generations and a 50% majority rule consensus tree.

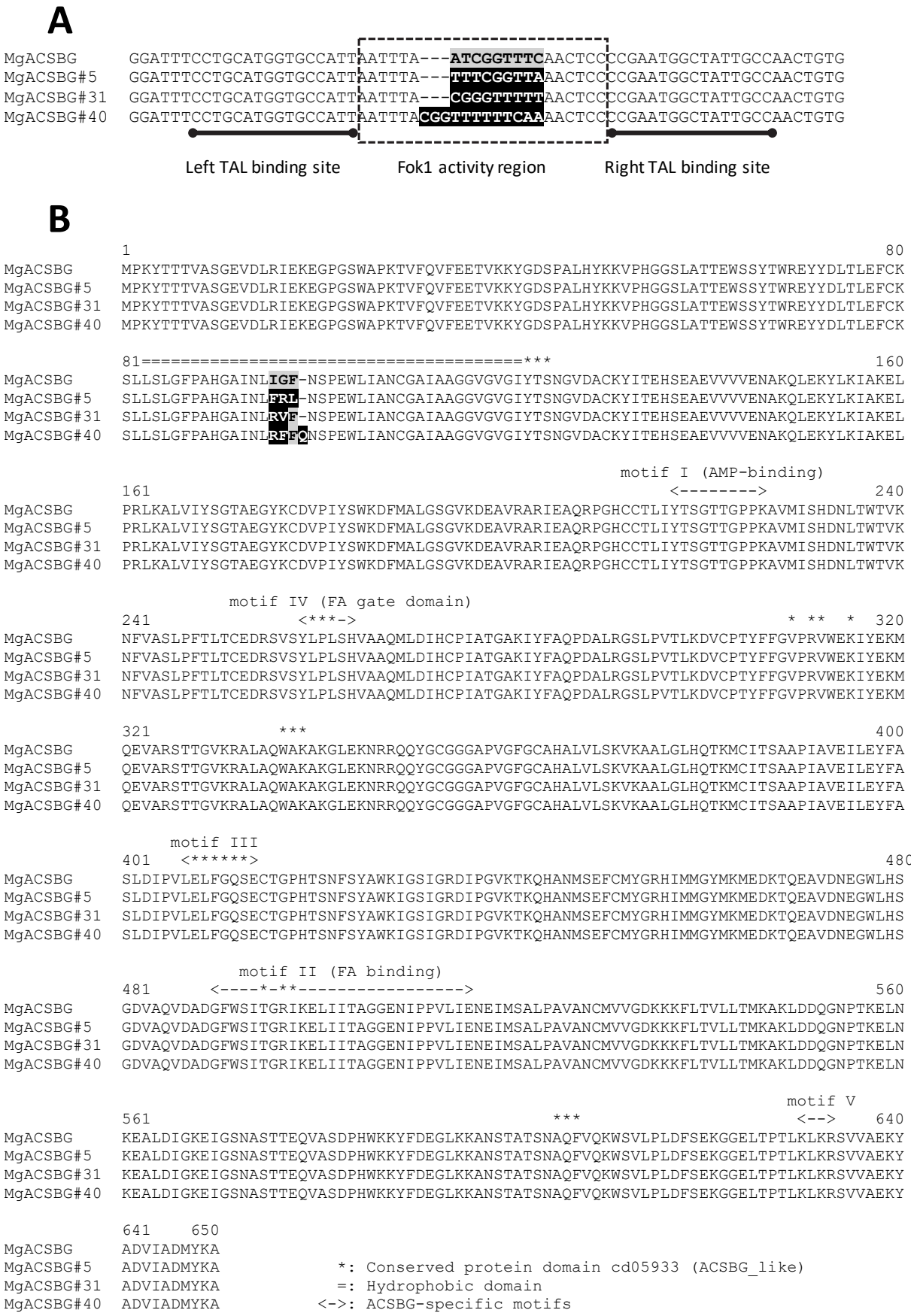

Figure 4: **MgACSBG mutants. (A)** Mutant selection. Following *M. gaditana* co-transformation with the two specifically designed TALE-N subunits, obtained clones were analyzed by treatment with a T7 endonuclease, to detect cleaved DNA at mismatched positions and assess occurrence of genome editing at the target locus. When this test allowed detecting a mutation, the cell population was sub-cloned onto a new selective plate and colonies arising from single cells were sequenced at the MgACSBG, inside the FokI activity region (frame) resulting in the appearance of novel codons. Three mutant lines harboring mutated endogenous *MgACSBG* are shown, called here MgACSBG#5, MgACSBG#31 and MgACSBG#40. Only two to three aminoacids were modified in the endogenous proteins. **(B)** Point mutations in MgACSBG#5, MgACSBG#31 and MgACSBG#40. In grey boxes, wild type (WT) residues at the TALE-N nucleotidic target; in black boxes, inserted mutations.

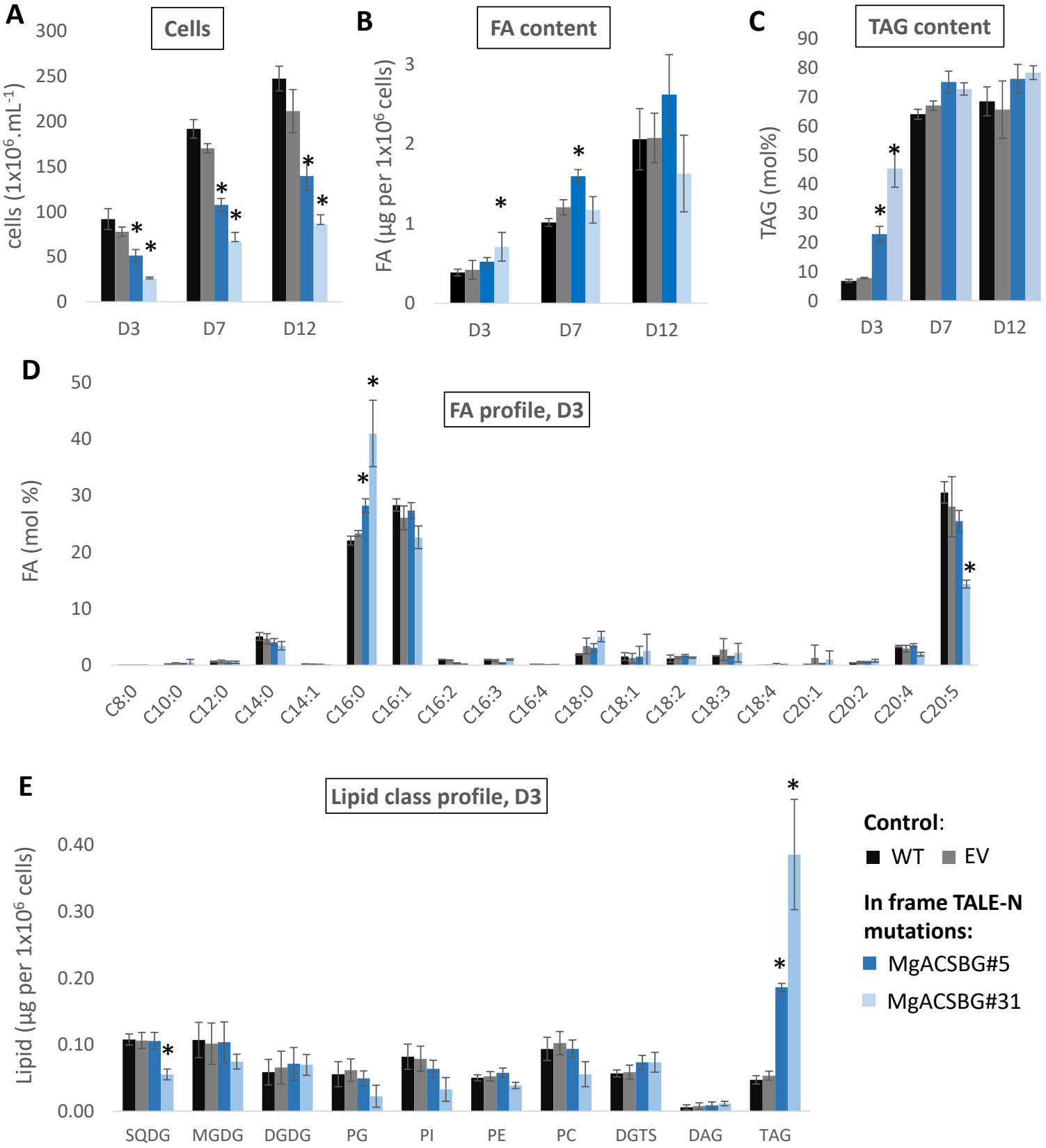

Figure 5: Compared analysis of MgACSBG#5 and MgACSBG#31 with untransformed wild type cells (WT) and cells transformed with an empty vector (EV). **(A)** Growth was measured by cell counting as described in the Method section at day 3, 7 and 12 following inoculation (D3, D7 and D12, respectively). D3 corresponds to nutrient replete cultivation, whereas D7 and D12 correspond to nitrogen-starved condition. **(B)** Fatty acid content per million cells at D3, D7 and D12 following inoculation. **(C)** Triacylglycerol content, in mol% of total glycerolipids, at D3, D7 and D12 following inoculation. **(D)** Fatty acid profile at D3. Total FAs were extracted and, following methanolysis, obtained FA methyl esters were analyzed and quantified by gas chromatography coupled with ion flame detection (GC-FID), as described in the Method section. **(E)** Glycerolipid profile at D3. Each glycerolipid class was analyzed by liquid chromatography coupled to tandem mass spectrometry (LC-MSMS) and quantified as described in the Methods section. DAG, diacylglycerol; DGDG, digalactosyldiacylglycerol; DGTS, diacylglyceryl-N,N,N-trimethylhomoserine; FA, fatty acid; MGDG, monogalactosyldiacylglycerol; PC, phosphatidylcholine; PE, phosphatidylethanolamine; PG, phosphatidylglycerol; PI, phosphatidylinositol; SQDG, sulfoquinovosyldiacylglycerol; TAG, triacylglycerol. Data are the average of 4 replicates. Error bars, standard deviation. (*), *P-value* < 0.05; student's t-test using WT as a reference.

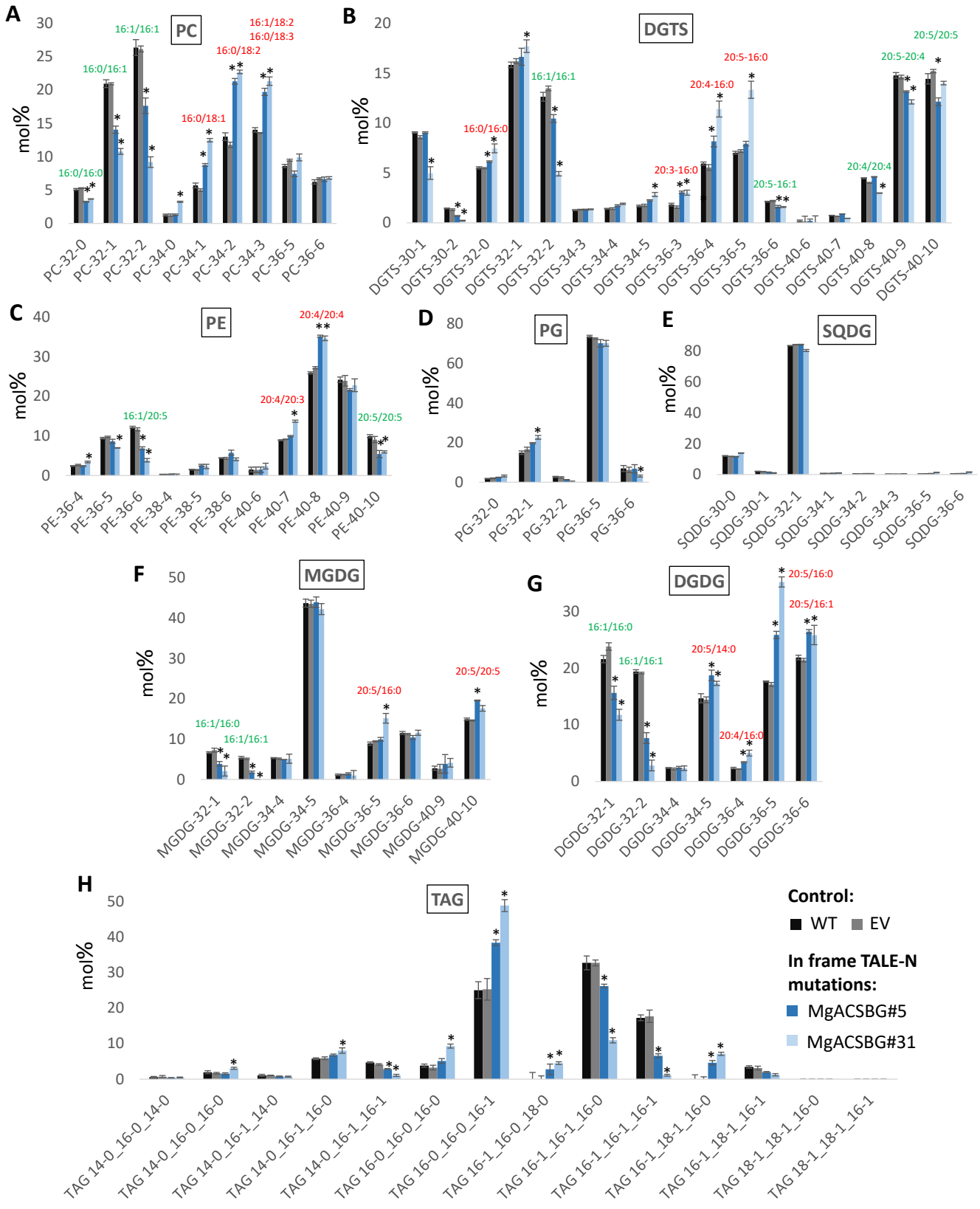

Figure 6: Comparison of the acyl profiles of glycerolipid classes in MgACSBG#5, MgACSBG#31, untransformed wild type cells (WT) and cells transformed with an empty vector (EV). (A) Phosphatidylcholine, PC. (B) Diacylglyceryl-N,N,N-trimethylhomoserine, DGTS. (C) Phosphatidylethanolamine, PE. (D) Phosphatidylglycerol, PG. (E) Sulfoquinovosyldiacylglycerol, SQDG. (F) Monogalactosyldiacylglycerol, MGDG. (G) Digalactosyldiacylglycerol, DGDG. (H) Triacylglycerol, TAG. Major molecular species corresponding to combined mass given in number of carbons and of double bonds are indicated, based on previous regioselective analysis of M. gaditana glycerolipids (Alboresi et al., 2016). Molecular species of which the proportion increases in the membrane lipids of MgACSBG#5 and MgACSBG#31 are shown in red, whereas those of which the proportion decreases are shown in green. Data are the average of 4 replicates and are given in mol%. Error bars, standard deviation. (*), P-value < 0.05; student's t-test using WT as a reference.

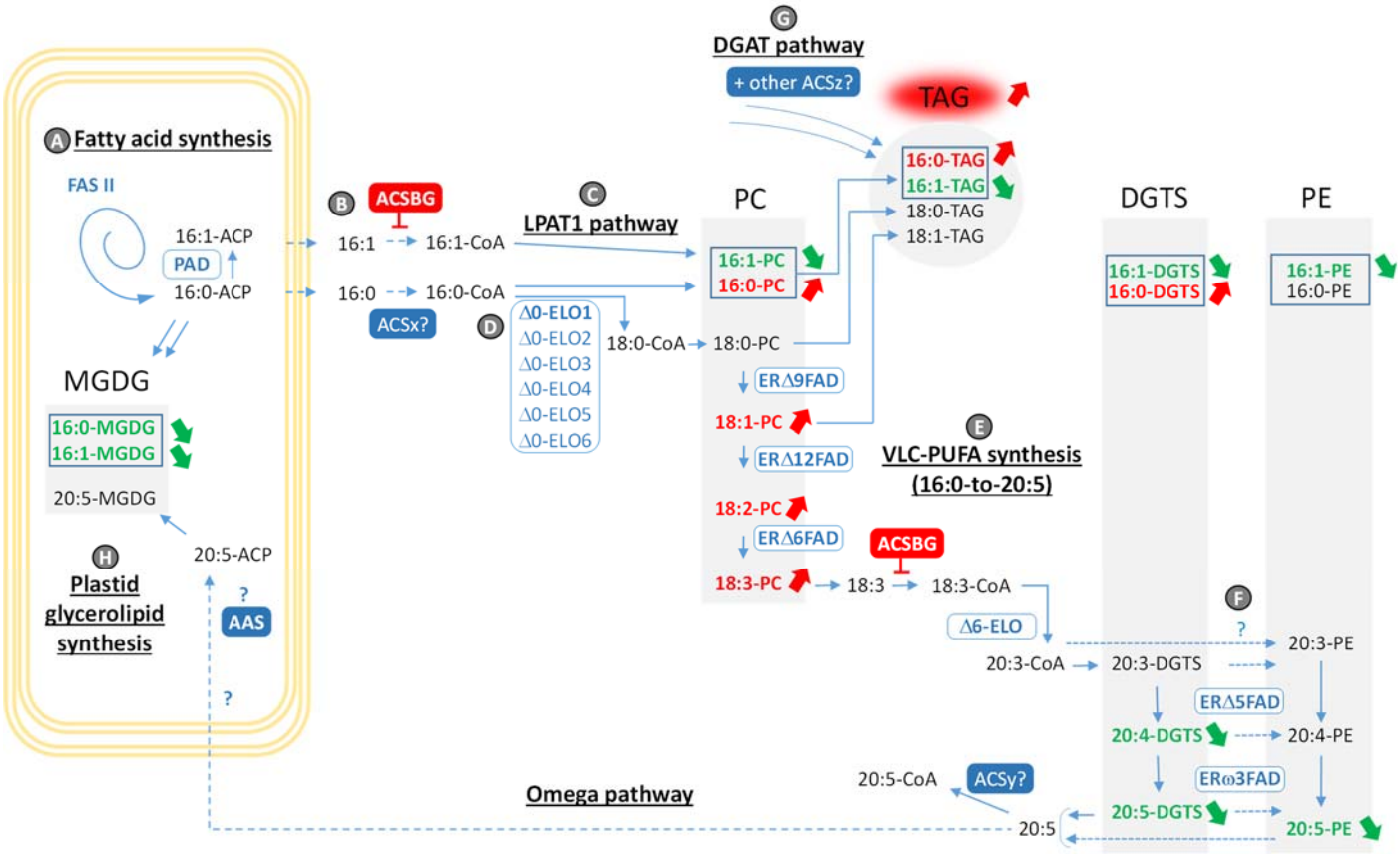

Figure 7: Model for ACSBG role in *M. gaditana*. The scheme shows the major fatty acids in major glycerolipid classes, i.e. PC, DGTS, PE and TAG in the ER, and MGDG in the plastid. Each membrane glycerolipid class is shown as a grey block. TAG is shown in a grey circle. **(A)** De novo synthesis of fatty acids (FAs) in the stroma of the plastid. The action of FA synthetase of type II (FAS II) leads to the production of 16:0-ACP, which can be desaturated by a palmitoyl ACP desaturase (PAD) into 16:1-ACP. These acyls can be exported to the cytosol, possibly as free fatty acids, through the four limiting membranes of the plastid. **(B)** ACSBG phenotype is consistent with a role in the production of 16:1-CoA. An unknown ACS isoforms (ACSx) catalyze the production of 16:0-CoA. **(C)** It was shown that 16:1 is incorporated at the sn-2 position of ER lipids via LPAT1 in *N. oceanica* (Nobusawa et al., 2017). Impairment of ACSBG alters this process. **(D)** It was shown that 16:0-CoA is elongated into 18:0-CoA by the action of D0-ELO isoforms, as a committing step in the 16:0-to-20:5 synthesis pathway (Dolch et al., 2017). **(E)** VLC-PUFA synthesis, starting by the 18:0-to-18:3 desaturation on PC, by the stepwise action of an ERD9FAD, an ERD12FAD and an ERD6FAD. Since PC accumulates 18 precursors (18:1 and 18:2) we consider that the mutants are likely impaired downstream, at the level of 18:3 elongation, leading therefore to the positioning of ACSBG at the level of 18:3-CoA production, feeding the Δ6-ELO isoform producing 20:3-CoA. Downstream processes, i.e. 20:3-to-20:5 desaturations occurring on DGTS would be consistently impaired, with a decrease in the end-product, 20:5. **(F)** Some 20:3-to-20:5 desaturation processes occurring in DGTS operate also in PE. The slowing down of 20:5 synthesis also occurs in PE. **(G)** As a result, following the mass action law, the slowing down occurring in the 16:0-to-20:5 pathway is expected to lead to an over-accumulation of 16:0-CoA. Excess 16:0-CoA can be stored into TAG, via the DGAT/Kennedy pathway. **(H)** An important assumption for this model is that a positive feedback is exerted on the plastid, exporting most its FAs, and explaining that the omega pathway is activated to provide sufficient 20:5 to plastid glycerolipids to compensate the lack of 16-carbon substrates. AAS, acyl-ACP synthetase; ACS, acyl-CoA synthetase; DGAT, diacylglycerol acyltransferase; DGTS, diacylglyceryl-N,N,N-trimethylhomoserine; FAD, fatty acid desaturase; MGDG, monogalactosyldiacylglycerol; PAD, palmitoyl ACP desaturase; PC, phosphatidylcholine; PE, phosphatidylethanolamine; TAG, triacylglycerol.

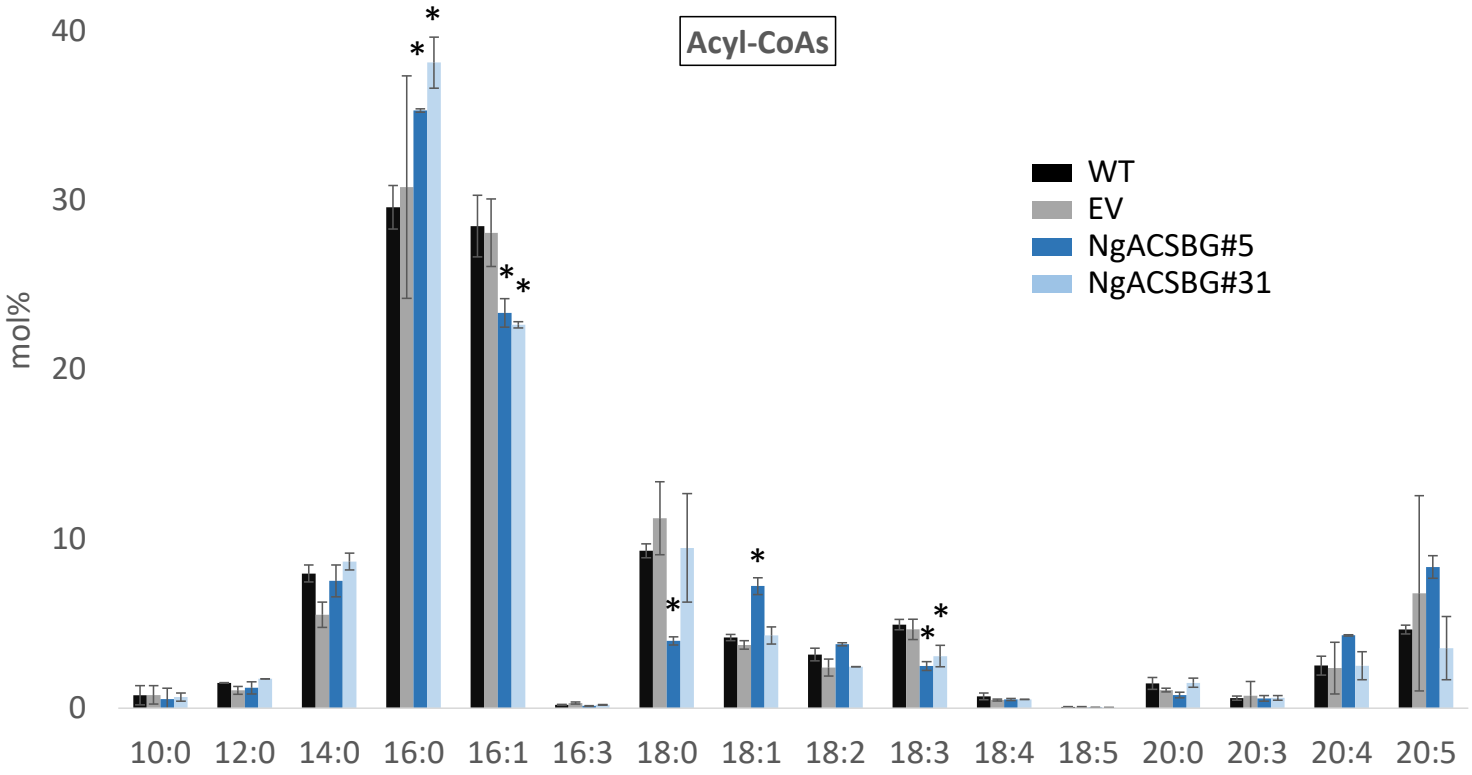

Figure 8: Comparison of the acyl-CoA profiles in MgACSBG#5, MgACSBG#31, untransformed wild type cells (WT) and cells transformed with an empty vector (EV). Cells were cultivated in nutrient replete conditions as described in the Method section (D3). Mass-spectrometry based analysis and data processing were performed by Rothamsted Research, UK. Data are the average of 2 replicates. Error bars, standard deviation. (*), P-value < 0.05; student's t-test using WT as a reference.

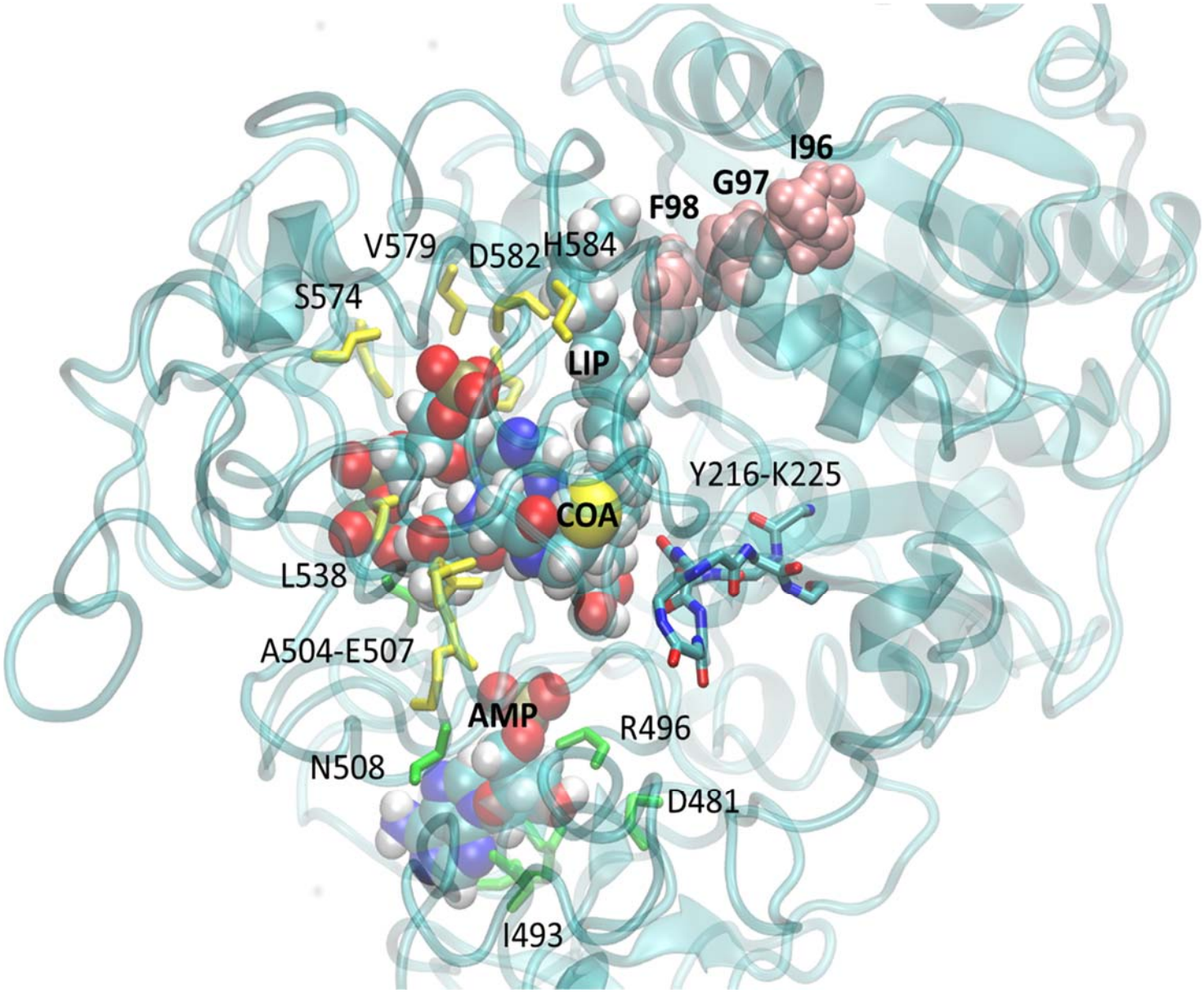

Figure 9. 3D model of MgACSBG bound to CoA, AMP and α-linolenic acid (18:3). Four models of MgACSBG were obtained based on similarity with acetyl- and acyl-CoA synthetase of known 3D structure, as described in the method section. The Mcons1 model of MgACSBG is shown with the visualization program VMD (Humphrey et al., 1996). The backbone of residues around AMP and CoA, listed in Supplemental Table S2A and S2B, are shown in licorice. The IGF triad is represented in pink (I96, G97, F98). The conserved Y216-K225 active site is shown in licorice mode. The position of IGF close to 18:3 is similar in all four MgACSBG models. Abbreviations: COA, Coenzyme A; AMP, adenosine monophosphate; LIP, α-linolenic acid.

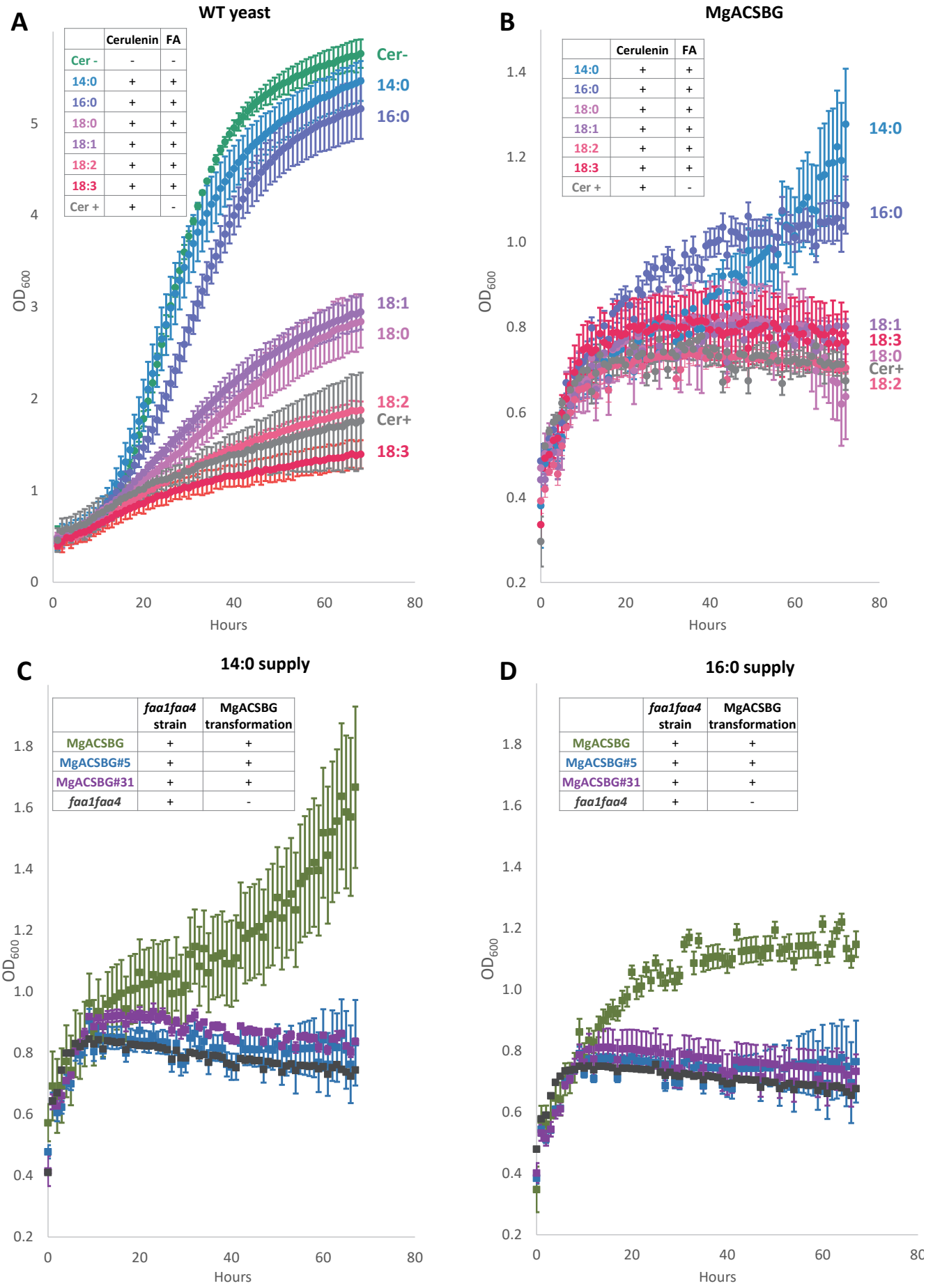

Figure 10. Growth complementation of yeast mutant defective in acyl-CoA activity by MgACSBG variants. (A) WT yeast strain growth curves in galactose medium (Cer-, green circles, positive control), with the addition of 22.5 µM cerulenin only (Cer+, grey circles, negative control), or with the addition of 22.5 µM cerulenin and 100 µM of the following free fatty acids, 14:0, 16:0, 18:0, 18:1, 18:2 and 18:3 (curves ranging from blue to red). **(B)** Growth curves of MgACSBG complemented *faa1Δfaa4Δ* double yeast mutant in galactose medium supplemented by 22.5 µM cerulenin and 100 µM of FA (curves ranging from blue to red). Medium with 22.5µM cerulenin but FA is used as a negative control (Cer+, grey circles). Average (+/- standard deviation) of biological (n = 3, independent clones) as well as technical (n = 3) replicates are presented. **(C)** and **(D)** Growth curves of the *faa1Δfaa4Δ* double mutant complemented with MgACSBG (green squares), MgACSBG#5 (blue squares), and MgACSBG#31 (purple squares) in presence of 22.5µM cerulenin and 100 µM 14:0 (C) or 16:0 (D). The *faa1Δfaa4Δ* double mutant without complementation is used as negative control and represented by grey circles. Average (+/- standard deviation) of biological (n = 3, independent clones) replicates are presented.

Parsed Citations

Abida H, Dolch LJ, Mei C, Villanova V, Conte M, Block MA, Finazzi G, Bastien O, Tirichine L, Bowler C, Rebeille F, Petroutsos D, Jouhet J, Marechal E (2015) Membrane glycerolipid remodeling triggered by nitrogen and phosphorus starvation in Phaeodactylum tricornutum. Plant Physiol 167: 118-136

Google Scholar: Author Only Title Only Author and Title

Abida H, Ruchaud S, Rios L, Humeau A, Probert I, De Vargas C, Bach S, Bowler C (2013) Bioprospecting marine plankton. Mar Drugs 11: 4594-4611

Google Scholar: Author Only Title Only Author and Title

Alboresi A, Perin G, Vitulo N, Diretto G, Block MA, Jouhet J, Meneghesso A, Valle G, Giuliano G, Marechal E, Morosinotto T (2016) Light Remodels Lipid Biosynthesis in Nannochloropsis gaditana by Modulating Carbon Partitioning Between Organelles. Plant Physiol

Google Scholar: Author Only Title Only Author and Title

Altschul SF, Gish W, Miller W, Myers EW, Lipman DJ (1990) Basic Local Alignment Search Tool. Journal of Molecular Biology 215: 403-410

Google Scholar: Author Only Title Only Author and Title

Bates PD, Fatihi A, Snapp AR, Carlsson AS, Browse J, Lu C (2012) Acyl editing and headgroup exchange are the major mechanisms that direct polyunsaturated fatty acid flux into triacylglycerols. Plant Physiol 160: 1530-1539

Google Scholar: Author Only Title Only Author and Title

Benning C (2008) A role for lipid trafficking in chloroplast biogenesis. Progress in Lipid Research 47: 381-389

Google Scholar: Author Only Title Only Author and Title

Benning C (2009) Mechanisms of lipid transport involved in organelle biogenesis in plant cells. Annu Rev Cell Dev Biol 25: 71-91

Google Scholar: Author Only Title Only Author and Title

Black PN, DiRusso CC (2007) Yeast acyl-CoA synthetases at the crossroads of fatty acid metabolism and regulation. Biochimica Et Biophysica Acta-Molecular and Cell Biology of Lipids 1771: 286-298

Google Scholar: Author Only Title Only Author and Title

Black PN, Zhang Q, Weimar JD, DiRusso CC (1997) Mutational analysis of a fatty acyl-coenzyme A synthetase signature motif identifies seven amino acid residues that modulate fatty acid substrate specificity. J Biol Chem 272: 4896-4903

Google Scholar: Author Only Title Only Author and Title

Botte CY, Yamaryo-Botte Y, Janouskovec J, Rupasinghe T, Keeling PJ, Crellin P, Coppel RL, Marechal E, McConville MJ, McFadden GI (2011) Identification of plant-like galactolipids in Chromera velia, a photosynthetic relative of malaria parasites. J Biol Chem 286: 29893-29903

Google Scholar: Author Only Title Only Author and Title

Boudiere L, Botte CY, Saidani N, Lajoie M, Marion J, Brehelin L, Yamaryo-Botte Y, Satiat-Jeunemaitre B, Breton C, Girard-Egrot A, Bastien O, Jouhet J, Falconet D, Block MA, Marechal E (2012) Galvestine-1, a novel chemical probe for the study of the glycerolipid homeostasis system in plant cells. Mol Biosyst 8: 2023-2035, 2014

Google Scholar: Author Only Title Only Author and Title

Boudiere L, Michaud M, Petroutsos D, Rebeille F, Falconet D, Bastien O, Roy S, Finazzi G, Rolland N, Jouhet J, Block MA, Marechal E (2014) Glycerolipids in photosynthesis: composition, synthesis and trafficking. Biochim Biophys Acta 1837: 470-480

Google Scholar: Author Only Title Only Author and Title

Brooks BR, Brooks CL, 3rd, Mackerell AD, Jr., Nilsson L, Petrella RJ, Roux B, Won Y, Archontis G, Bartels C, Boresch S, Caflisch A, Caves L, Cui Q, Dinner AR, Feig M, Fischer S, Gao J, Hodoscek M, Im W, Kuczera K, Lazaridis T, Ma J, Ovchinnikov V, Paci E, Pastor RW, Post CB, Pu JZ, Schaefer M, Tidor B, Venable RM, Woodcock HL, Wu X, Yang W, York DM, Karplus M (2009) CHARMM: the biomolecular simulation program. J Comput Chem 30: 1545-1614

Google Scholar: Author Only Title Only Author and Title

Buchan DW, Minneci F, Nugent TC, Bryson K, Jones DT (2013) Scalable web services for the PSIPRED Protein Analysis Workbench. Nucleic Acids Res 41: W349-357

Google Scholar: Author Only Title Only Author and Title

Burley SK, Berman HM, Bhikadiya C, Bi CX, Chen L, Di Costanzo L, Christie C, Duarte JM, Dutta S, Feng ZK, Ghosh S, Goodsell DS, Green RK, Guranovic V, Guzenko D, Hudson BP, Liang YH, Lowe R, Peisach E, Periskova I, Randle C, Rose A, Sekharan M, Shao CH, Tao YP, Valasatava Y, Voigt M, Westbrook J, Young J, Zardecki C, Zhuravleva M, Kurisu G, Nakamura H, Kengaku Y, Cho H, Sato J, Kim JY, Ikegawa Y, Nakagawa A, Yamashita R, Kudou T, Bekker GJ, Suzuki H, Iwata T, Yokochi M, Kobayashi N, Fujiwara T, Velankar S, Kleywegt GJ, Anyango S, Armstrong DR, Berrisford JM, Conroy MJ, Dana JM, Deshpande M, Gane P, Gaborova R, Gupta D, Gutmanas A, Koca J, Mak L, Mir S, Mukhopadhyay A, Nadzirin N, Nair S, Patwardhan A, Paysan-Lafosse T, Pravda L, Salih O, Sehnal D, Varadi M, Varekova R, Markley JL, Hoch JC, Romero PR, Baskaran K, Maziuk D, Ulrich EL, Wedell JR, Yao HY, Livny M, Ioannidis YE, Consortium W, Japan PDB (2019) Protein Data Bank: the single global archive for 3D macromolecular structure data. Nucleic Acids Research 47: D520-D528

Google Scholar: Author Only Title Only Author and Title

Buseman CM, Tamura P, Sparks AA, Baughman EJ, Maatta S, Zhao J, Roth MR, Esch SW, Shah J, Williams TD, Welti R (2006) Wounding stimulates the accumulation of glycerolipids containing oxophytodienoic acid and dinor-oxophytodienoic acid in Arabidopsis leaves. Plant Physiol 142: 28-39
Google Scholar: Author Only Title Only Author and Title

Camacho-Rodriguez J, Ceron-Garcia MC, Fernandez-Sevilla JM, Molina-Grima E (2015) Genetic algorithm for the medium optimization of the microalga Nannochloropsis gaditana cultured to aquaculture. Bioresour Technol 177: 102-109
Google Scholar: Author Only Title Only Author and Title

Camacho-Rodriguez J, Ceron-Garcia MC, Gonzalez-Lopez CV, Fernandez-Sevilla JM, Contreras-Gomez A, Molina-Grima E (2013) A low-cost culture medium for the production of Nannochloropsis gaditana biomass optimized for aquaculture. Bioresour Technol 144: 57-66
Google Scholar: Author Only Title Only Author and Title

Camacho-Rodriguez J, Gonzalez-Cespedes AM, Ceron-Garcia MC, Fernandez-Sevilla JM, Acien-Fernandez FG, Molina-Grima E (2014) A quantitative study of eicosapentaenoic acid (EPA) production by Nannochloropsis gaditana for aquaculture as a function of dilution rate, temperature and average irradiance. Appl Microbiol Biotechnol 98: 2429-2440
Google Scholar: Author Only Title Only Author and Title

Castresana J (2000) Selection of conserved blocks from multiple alignments for their use in phylogenetic analysis. Mol Biol Evol 17: 540-552
Google Scholar: Author Only Title Only Author and Title

Cavalier-Smith T (2018) Kingdom Chromista and its eight phyla: a new synthesis emphasising periplastid protein targeting, cytoskeletal and periplastid evolution, and ancient divergences. Protoplasma 255: 297-357
Google Scholar: Author Only Title Only Author and Title

Chen CY, Chen YC, Huang HC, Huang CC, Lee WL, Chang JS (2013) Engineering strategies for enhancing the production of eicosapentaenoic acid (EPA) from an isolated microalga Nannochloropsis oceanica CY2. Bioresour Technol 147: 160-167
Google Scholar: Author Only Title Only Author and Title

Claire D'Andre H, Paul W, Shen X, Jia X, Zhang R, Sun L, Zhang X (2013) Identification and characterization of genes that control fat deposition in chickens. J Anim Sci Biotechnol 4: 43
Google Scholar: Author Only Title Only Author and Title

Coleman RA, Lewin TM, Van Horn CG, Gonzalez-Baro MR (2002) Do long-chain acyl-CoA synthetases regulate fatty acid entry into synthetic versus degradative pathways? J Nutr 132: 2123-2126
Google Scholar: Author Only Title Only Author and Title

Degraeve-Guilbault C, Brehelin C, Haslam R, Sayanova O, Marie-Luce G, Jouhet J, Corellou F (2017) Glycerolipid Characterization and Nutrient Deprivation-Associated Changes in the Green Picoalga Ostreococcus tauri. Plant Physiol 173: 2060-2080
Google Scholar: Author Only Title Only Author and Title

Deme B, Cataye C, Block MA, Marechal E, Jouhet J (2014) Contribution of galactoglycerolipids to the 3-dimensional architecture of thylakoids. FASEB J 28: 3373-3383
Google Scholar: Author Only Title Only Author and Title

Dereeper A, Guignon V, Blanc G, Audic S, Buffet S, Chevenet F, Dufayard JF, Guindon S, Lefort V, Lescot M, Claverie JM, Gascuel O (2008) Phylogeny.fr: robust phylogenetic analysis for the non-specialist. Nucleic Acids Res 36: W465-469
Google Scholar: Author Only Title Only Author and Title

Dolch LJ, Lupette J, Tourcier G, Bedhomme M, Collin S, Magneschi L, Conte M, Seddiki K, Richard C, Corre E, Fourage L, Laeuffer F, Richards R, Reith M, Rebeille F, Jouhet J, McGinn P, Marechal E (2017) Nitric Oxide Mediates Nitrite-Sensing and Acclimation and Triggers a Remodeling of Lipids. Plant Physiol 175: 1407-1423
Google Scholar: Author Only Title Only Author and Title

Dolch LJ, Marechal E (2015) Inventory of fatty acid desaturases in the pennate diatom Phaeodactylum tricornutum. Mar Drugs 13: 1317-1339
Google Scholar: Author Only Title Only Author and Title

Dolch LJ, Rak C, Perin G, Tourcier G, Broughton R, Leterrier M, Morosinotto T, Tellier F, Faure JD, Falconet D, Jouhet J, Sayanova O, Beaudoin F, Marechal E (2017) A Palmitic Acid Elongase Affects Eicosapentaenoic Acid and Plastidial Monogalactosyldiacylglycerol Levels in Nannochloropsis. Plant Physiol 173: 742-759
Google Scholar: Author Only Title Only Author and Title

Edgar RC (2004) MUSCLE: multiple sequence alignment with high accuracy and high throughput. Nucleic Acids Res 32: 1792-1797
Google Scholar: Author Only Title Only Author and Title

Faergeman NJ, Black PN, Zhao XD, Knudsen J, DiRusso CC (2001) The acyl-CoA synthetases encoded within FAA1 and FAA4 in Saccharomyces cerevisiae function as components of the fatty acid transport system linking import, activation, and intracellular utilization. Journal of Biological Chemistry 276: 37051-37059
Google Scholar: Author Only Title Only Author and Title

Fawley MW, Jameson I, Fawley KP (2015) The phylogeny of the genus Nannochloropsis (Monodopsidaceae, Eustigmatophyceae), with descriptions of N. australis sp. nov. and Microchloropsis gen. nov. Phycologia 54: 545-552
Google Scholar: Author Only Title Only Author and Title

Flori S, Jouneau P-H, Finazzi G, Maréchal E, Falconet D (2016) Ultrastructure of the Periplastidial Compartment of the Diatom Phaeodactylum tricornutum. Protist 167: 254-267
Google Scholar: Author Only Title Only Author and Title

Fussy Z, Obornik M (2018) Complex Endosymbioses I: From Primary to Complex Plastids, Multiple Independent Events. Methods Mol Biol 1829: 17-35
Google Scholar: Author Only Title Only Author and Title

Gahloth D, Dunstan MS, Quaglia D, Klumbys E, Lockhart-Cairns MP, Hill AM, Derrington SR, Scrutton NS, Turner NJ, Leys D (2017) Structures of carboxylic acid reductase reveal domain dynamics underlying catalysis. Nat Chem Biol 13: 975-981
Google Scholar: Author Only Title Only Author and Title

Gietz RD, Schiestl RH (2007) Large-scale high-efficiency yeast transformation using the LiAc/SS carrier DNA/PEG method. Nature Protocols 2: 38-41
Google Scholar: Author Only Title Only Author and Title

Gulick AM, Starai VJ, Horswill AR, Homick KM, Escalante-Semerena JC (2003) The 1.75 A crystal structure of acetyl-CoA synthetase bound to adenosine-5'-propylphosphate and coenzyme A. Biochemistry 42: 2866-2873
Google Scholar: Author Only Title Only Author and Title

Haynes CA, Allegood JC, Sims K, Wang EW, Sullards MC, Merrill AH, Jr. (2008) Quantitation of fatty acyl-coenzyme As in mammalian cells by liquid chromatography-electrospray ionization tandem mass spectrometry. J Lipid Res 49: 1113-1125
Google Scholar: Author Only Title Only Author and Title

Hisanaga Y, Ago H, Nakagawa N, Hamada K, Ida K, Yamamoto M, Hori T, Arii Y, Sugahara M, Kuramitsu S, Yokoyama S, Miyano M (2004) Structural basis of the substrate-specific two-step catalysis of long chain fatty acyl-CoA synthetase dimer. J Biol Chem 279: 31717-31726
Google Scholar: Author Only Title Only Author and Title

Horn PJ, Benning C (2016) The plant lipidome in human and environmental health. Science 353: 1228-1232
Google Scholar: Author Only Title Only Author and Title

Huang TT, Hwang JK, Chen CH, Chu CS, Lee CW, Chen CC (2015) (PS)2: protein structure prediction server version 3.0. Nucleic Acids Res 43: W338-342
Google Scholar: Author Only Title Only Author and Title

Huelsenbeck JP, Ronquist F (2001) MRBAYES: Bayesian inference of phylogenetic trees. Bioinformatics 17: 754-755
Google Scholar: Author Only Title Only Author and Title

Humphrey W, Dalke A, Schulten K (1996) VMD: visual molecular dynamics. J Mol Graph 14: 33-38, 27-38
Google Scholar: Author Only Title Only Author and Title

Hurlock AK, Wang K, Takeuchi T, Horn PJ, Benning C (2018) In vivo lipid 'tag and track' approach shows acyl editing of plastid lipids and chloroplast import of phosphatidylglycerol precursors in Arabidopsis thaliana. Plant J 95: 1129-1139
Google Scholar: Author Only Title Only Author and Title

Iwai M, Hori K, Sasaki-Sekimoto Y, Shimojima M, Ohta H (2015) Manipulation of oil synthesis in Nannochloropsis strain NIES-2145 with a phosphorus starvation-inducible promoter from Chlamydomonas reinhardtii. Front Microbiol 6: 912
Google Scholar: Author Only Title Only Author and Title

Johnson DR, Knoll LJ, Levin DE, Gordon JI (1994) Saccharomyces cerevisiae contains four fatty acid activation (FAA) genes: an assessment of their role in regulating protein N-myristoylation and cellular lipid metabolism. J Cell Biol 127: 751-762
Google Scholar: Author Only Title Only Author and Title

Johnson DR, Knoll LJ, Rowley N, Gordon JI (1994) Genetic analysis of the role of Saccharomyces cerevisiae acyl-CoA synthetase genes in regulating protein N-myristoylation. J Biol Chem 269: 18037-18046
Google Scholar: Author Only Title Only Author and Title

Jouhet J, Lupette J, Clerc O, Magneschi L, Bedhomme M, Collin S, Roy S, Maréchal E, Rébeillé F (2017) LC-MS/MS versus TLC plus GC methods: Consistency of glycerolipid and fatty acid profiles in microalgae and higher plant cells and effect of a nitrogen starvation. PLOS ONE 12: e0182423
Google Scholar: Author Only Title Only Author and Title

Jouhet J, Marechal E, Bligny R, Joyard J, Block MA (2003) Transient increase of phosphatidylcholine in plant cells in response to phosphate deprivation. FEBS Lett 544: 63-68
Google Scholar: Author Only Title Only Author and Title

Kallberg M, Wang HP, Wang S, Peng J, Wang ZY, Lu H, Xu JB (2012) Template-based protein structure modeling using the RaptorX web server. Nature Protocols 7: 1511-1522
Google Scholar: Author Only Title Only Author and Title

Kanehisa M, Goto S, Kawashima S, Nakaya A (2002) The KEGG databases at GenomeNet. Nucleic Acids Res 30: 42-46
Google Scholar: Author Only Title Only Author and Title

Kang NK, Jeon S, Kwon S, Koh HG, Shin SE, Lee B, Choi GG, Yang JW, Jeong BR, Chang YK (2015) Effects of overexpression of a bHLH transcription factor on biomass and lipid production in Nannochloropsis salina. Biotechnol Biofuels 8: 200
Google Scholar: Author Only Title Only Author and Title

Kelley LA, Mezulis S, Yates CM, Wass MN, Sternberg MJ (2015) The Phyre2 web portal for protein modeling, prediction and analysis. Nat Protoc 10: 845-858
Google Scholar: Author Only Title Only Author and Title

Kochan G, Pilka ES, von Delft F, Oppermann U, Yue WW (2009) Structural Snapshots for the Conformation-dependent Catalysis by Human Medium-chain Acyl-coenzyme A Synthetase ACSM2A. Journal of Molecular Biology 388: 997-1008
Google Scholar: Author Only Title Only Author and Title

LaBrant E, Barnes AC, Roston RL (2018) Lipid transport required to make lipids of photosynthetic membranes. Photosynth Res 138: 345-360
Google Scholar: Author Only Title Only Author and Title

Laskowski RA, Macarthur MW, Moss DS, Thornton JM (1993) Procheck - a Program to Check the Stereochemical Quality of Protein Structures. Journal of Applied Crystallography 26: 283-291
Google Scholar: Author Only Title Only Author and Title

Li-Beisson Y, Neunzig J, Lee Y, Philippar K (2017) Plant membrane-protein mediated intracellular traffic of fatty acids and acyl lipids. Curr Opin Plant Biol 40: 138-146
Google Scholar: Author Only Title Only Author and Title

Li-Beisson Y, Shorrosh B, Beisson F, Andersson MX, Arondel V, Bates PD, Baud S, Bird D, Debono A, Durrett TP, Franke RB, Graham IA, Katayama K, Kelly AA, Larson T, Markham JE, Miquel M, Molina I, Nishida I, Rowland O, Samuels L, Schmid KM, Wada H, Welti R, Xu C, Zallot R, Ohlrogge J (2010) Acyl-lipid metabolism. In The Arabidopsis Book, Ed 2010/01/01 Vol 8, p e0133
Google Scholar: Author Only Title Only Author and Title

Li-Beisson Y, Thelen JJ, Fedosejevs E, Harwood JL (2019) The lipid biochemistry of eukaryotic algae. Prog Lipid Res 74: 31-68
Google Scholar: Author Only Title Only Author and Title

Li N, Gugel IL, Giavalisco P, Zeisler V, Schreiber L, Soll J, Philippar K (2015) FAX1, a novel membrane protein mediating plastid fatty acid export. PLoS Biol 13: e1002053
Google Scholar: Author Only Title Only Author and Title

Li N, Xu C, Li-Beisson Y, Philippar K (2016) Fatty Acid and Lipid Transport in Plant Cells. Trends Plant Sci 21: 145-158
Google Scholar: Author Only Title Only Author and Title

Lopes-Marques M, Machado AM, Ruivo R, Fonseca E, Carvalho E, Castro LFC (2018) Expansion, retention and loss in the Acyl-CoA synthetase "Bubblegum" (Acsbg) gene family in vertebrate history. Gene 664: 111-118
Google Scholar: Author Only Title Only Author and Title

Lupette J, Jaussaud A, Seddiki K, Morabito C, Brugiere S, Schaller H, Kuntz M, Putaux JL, Jouneau PH, Rebellle F, Falconet D, Coute Y, Jouhet J, Tardif M, Salvaing J, Marechal E (2019) The architecture of lipid droplets in the diatom Phaeodactylum tricornutum. Algal Research-Biomass Biofuels and Bioproducts 38
Google Scholar: Author Only Title Only Author and Title

Ma AC, Chen Y, Blackburn PR, Ekker SC (2016) TALEN-Mediated Mutagenesis and Genome Editing. Methods Mol Biol 1451: 17-30
Google Scholar: Author Only Title Only Author and Title

Ma Y, Wang Z, Yu C, Yin Y, Zhou G (2014) Evaluation of the potential of 9 Nannochloropsis strains for biodiesel production. Bioresour Technol 167: 503-509
Google Scholar: Author Only Title Only Author and Title

Malzahn A, Lowder L, Qi Y (2017) Plant genome editing with TALEN and CRISPR. Cell Biosci 7: 21
Google Scholar: Author Only Title Only Author and Title

Mashek DG, Li LO, Coleman RA (2007) Long-chain acyl-CoA synthetases and fatty acid channeling. Future Lipidol 2: 465-476
Google Scholar: Author Only Title Only Author and Title

Mashek DG, McKenzie MA, Van Horn CG, Coleman RA (2006) Rat long chain acyl-CoA synthetase 5 increases fatty acid uptake and partitioning to cellular triacylglycerol in McArdle-RH7777 cells. J Biol Chem 281: 945-950
Google Scholar: Author Only Title Only Author and Title

Menard GN, Bryant FM, Kelly AA, Craddock CP, Lavagi I, Hassani-Pak K, Kurup S, Eastmond PJ (2018) Natural variation in acyl editing is a determinant of seed storage oil composition. Sci Rep 8: 17346
Google Scholar: Author Only Title Only Author and Title

Meng Y, Jiang J, Wang H, Cao X, Xue S, Yang Q, Wang W (2015) The characteristics of TAG and EPA accumulation in Nannochloropsis

oceanica IMET1 under different nitrogen supply regimes. Bioresour Technol 179: 483-489
Google Scholar: Author Only Title Only Author and Title

Min KT, Benzer S (1999) Preventing neurodegeneration in the Drosophila mutant bubblegum. Science 284: 1985-1988
Google Scholar: Author Only Title Only Author and Title

Mirabello C, Pollastri G (2013) Porter, PaleAle 4.0: high-accuracy prediction of protein secondary structure and relative solvent accessibility. Bioinformatics 29: 2056-2058
Google Scholar: Author Only Title Only Author and Title

Moriya-Sato A, Hida A, Inagawa-Ogashiwa M, Wada MR, Sugiyama K, Shimizu J, Yabuki T, Seyama Y, Hashimoto N (2000) Novel acyl-CoA synthetase in adrenoleukodystrophy target tissues. Biochem Biophys Res Commun 279: 62-68
Google Scholar: Author Only Title Only Author and Title

Murakami H, Nobusawa T, Hori K, Shimojima M, Ohta H (2018) Betaine Lipid Is Crucial for Adapting to Low Temperature and Phosphate Deficiency in Nannochloropsis. Plant Physiol 177: 181-193
Google Scholar: Author Only Title Only Author and Title

Nobusawa T, Hori K, Mori H, Kurokawa K, Ohta H (2017) Differently localized lysophosphatidic acid acyltransferases crucial for triacylglycerol biosynthesis in the oleaginous alga Nannochloropsis. Plant J 90: 547-559
Google Scholar: Author Only Title Only Author and Title

Pei Z, Oey NA, Zuidervaart MM, Jia Z, Li Y, Steinberg SJ, Smith KD, Watkins PA (2003) The acyl-CoA synthetase "bubblegum" (lipidosin): further characterization and role in neuronal fatty acid beta-oxidation. J Biol Chem 278: 47070-47078
Google Scholar: Author Only Title Only Author and Title

Petroutsos D, Amiar S, Abida H, Dolch LJ, Bastien O, Rebeille F, Jouhet J, Falconet D, Block MA, McFadden GI, Bowler C, Botte C, Marechal E (2014) Evolution of galactoglycerolipid biosynthetic pathways--from cyanobacteria to primary plastids and from primary to secondary plastids. Prog Lipid Res 54: 68-85
Google Scholar: Author Only Title Only Author and Title

Poliner E, Farre EM, Benning C (2018) Advanced genetic tools enable synthetic biology in the oleaginous microalgae Nannochloropsis sp. Plant Cell Rep 37: 1383-1399
Google Scholar: Author Only Title Only Author and Title

Radakovits R, Jinkerson RE, Fuerstenberg SI, Tae H, Settlage RE, Boore JL, Posewitz MC (2012) Draft genome sequence and genetic transformation of the oleaginous alga Nannochloropis gaditana. Nat Commun 3: 686
Google Scholar: Author Only Title Only Author and Title

Rainteau D, Humbert L, Delage E, Vergnolle C, Cantrel C, Maubert MA, Lanfranchi S, Maldiney R, Collin S, Wolf C, Zachowski A, Ruelland E (2012) Acyl chains of phospholipase D transphosphatidylation products in Arabidopsis cells: a study using multiple reaction monitoring mass spectrometry. PLoS One 7: e41985
Google Scholar: Author Only Title Only Author and Title

Ramachandran GN, Ramakrishnan C, Sasisekharan V (1963) Stereochemistry of polypeptide chain configurations. J Mol Biol 7: 95-99
Google Scholar: Author Only Title Only Author and Title

Ronquist F, Teslenko M, van der Mark P, Ayres DL, Darling A, Hohna S, Larget B, Liu L, Suchard MA, Huelsenbeck JP (2012) MrBayes 3.2: efficient Bayesian phylogenetic inference and model choice across a large model space. Syst Biol 61: 539-542
Google Scholar: Author Only Title Only Author and Title

Sali A, Blundell TL (1993) Comparative protein modelling by satisfaction of spatial restraints. J Mol Biol 234: 779-815
Google Scholar: Author Only Title Only Author and Title

Sanjana NE, Cong L, Zhou Y, Cunniff MM, Feng G, Zhang F (2012) A transcription activator-like effector toolbox for genome engineering. Nat Protoc 7: 171-192
Google Scholar: Author Only Title Only Author and Title

Sayanova O, Mimouni V, Ulmann L, Morant-Manceau A, Pasquet V, Schoefs B, Napier JA (2017) Modulation of lipid biosynthesis by stress in diatoms. Philos Trans R Soc Lond B Biol Sci 372
Google Scholar: Author Only Title Only Author and Title

Sigrist CJ, de Castro E, Cerutti L, Cuche BA, Hulo N, Bridge A, Bougueleret L, Xenarios I (2013) New and continuing developments at PROSITE. Nucleic Acids Res 41: D344-347
Google Scholar: Author Only Title Only Author and Title

Simionato D, Block MA, La Rocca N, Jouhet J, Marechal E, Finazzi G, Morosinotto T (2013) The response of Nannochloropsis gaditana to nitrogen starvation includes de novo biosynthesis of triacylglycerols, a decrease of chloroplast galactolipids, and reorganization of the photosynthetic apparatus. Eukaryot Cell 12: 665-676
Google Scholar: Author Only Title Only Author and Title

Song SY, Kato C, Adachi E, Moriya-Sato A, Inagawa-Ogashiwa M, Umeda R, Hashimoto N (2007) Expression of an acyl-CoA synthetase, lipidosin, in astrocytes of the murine brain and its up-regulation during remyelination following cuprizone-induced demyelination. J Neurosci Res 85: 3586-3597

Google Scholar: Author Only Title Only Author and Title

Song YF, DiMaio F, Wang RYR, Kim D, Miles C, Brunette TJ, Thompson J, Baker D (2013) High-Resolution Comparative Modeling with RosettaCM. Structure 21: 1735-1742
Google Scholar: Author Only Title Only Author and Title

Steinberg SJ, Morgenthaler J, Heinzer AK, Smith KD, Watkins PA (2000) Very long-chain acyl-CoA synthetases. Human "bubblegum" represents a new family of proteins capable of activating very long-chain fatty acids. J Biol Chem 275: 35162-35169
Google Scholar: Author Only Title Only Author and Title

Van Vooren G, Le Grand F, Legrand J, Cuine S, Peltier G, Pruvost J (2012) Investigation of fatty acids accumulation in Nannochloropsis oculata for biodiesel application. Bioresour Technol 124: 421-432
Google Scholar: Author Only Title Only Author and Title

Vieler A, Wu G, Tsai CH, Bullard B, Cornish AJ, Harvey C, Reca IB, Thornburg C, Achawanantakun R, Buehl CJ, Campbell MS, Cavalier D, Childs KL, Clark TJ, Deshpande R, Erickson E, Armenia Ferguson A, Handee W, Kong Q, Li X, Liu B, Lundback S, Peng C, Roston RL, Sanjaya, Simpson JP, Terbush A, Warakanont J, Zauner S, Farre EM, Hegg EL, Jiang N, Kuo MH, Lu Y, Niyogi KK, Ohlrogge J, Osteryoung KW, Shachar-Hill Y, Sears BB, Sun Y, Takahashi H, Yandell M, Shiu SH, Benning C (2012) Genome, functional gene annotation, and nuclear transformation of the heterokont oleaginous alga Nannochloropsis oceanica CCMP1779. PLoS Genet 8: e1003064
Google Scholar: Author Only Title Only Author and Title

Waterhouse A, Bertoni M, Bienert S, Studer G, Tauriello G, Gumienny R, Heer FT, de Beer TAP, Rempfer C, Bordoli L, Lepore R, Schwede T (2018) SWISS-MODEL: homology modelling of protein structures and complexes. Nucleic Acids Res 46: W296-W303
Google Scholar: Author Only Title Only Author and Title

Watkins PA, Maiguel D, Jia Z, Pevsner J (2007) Evidence for 26 distinct acyl-coenzyme A synthetase genes in the human genome. J Lipid Res 48: 2736-2750
Google Scholar: Author Only Title Only Author and Title

Wilson D, Pethica R, Zhou YD, Talbot C, Vogel C, Madera M, Chothia C, Gough J (2009) SUPERFAMILY-sophisticated comparative genomics, data mining, visualization and phylogeny. Nucleic Acids Research 37: D380-D386
Google Scholar: Author Only Title Only Author and Title

Yachdav G, Kloppmann E, Kajan L, Hecht M, Goldberg T, Hamp T, Honigschmid P, Schafferhans A, Roos M, Bernhofer M, Richter L, Ashkenazy H, Punta M, Schlessinger A, Bromberg Y, Schneider R, Vriend G, Sander C, Ben-Tal N, Rost B (2014) PredictProtein--an open resource for online prediction of protein structural and functional features. Nucleic Acids Res 42: W337-343
Google Scholar: Author Only Title Only Author and Title

Zhang Y (2009) I-TASSER: fully automated protein structure prediction in CASP8. Proteins 77 Suppl 9: 100-113
Google Scholar: Author Only Title Only Author and Title

Zoete V, Cuendet MA, Grosdidier A, Michielin O (2011) SwissParam: a fast force field generation tool for small organic molecules. J Comput Chem 32: 2359-2368
Google Scholar: Author Only Title Only Author and Title